SYNAPTOTAGMIN SIGNAL PROPAGATION:
A MODEL SYSTEM FOR FUNCTIONAL COOPERATIVITY AT THE MEMBRANE

A THESIS SUBMITTED TO THE FACULTY OF THE GRADUATE SCHOOL OF THE UNIVERSITY OF MINNESOTA BY

Michael E. Fealey

IN PARTIAL FULFILLMENT OF THE REQUIREMENTS FOR THE DEGREE OF MASTER OF SCIENCE

Dr. Anne Hinderliter

June, 2013

Acknowledgments

Thanks are owed to Dr. Anne Hinderliter for her patience, encouraging career advice, and reserved judgment. Without her mentoring and support, the work presented here would not have been possible. I am also indebted to my former fellow graduate students: Jacob W. Gauer (for his training in protein denaturation and unbiased ear) and Samantha R. Jaworski (without whom I would not have found the strength to carry on at times). I would also like to thank Dr. R. Bryan Sutton (who was always willing to provide advice and read and revise manuscript drafts) and Kamakshi Nayak (who did the molecular biology and purified a substantial portion of the protein used for this thesis). I would also like to thank Komemba Lohese, Anne Rice, Ryan Mahling, and Heathere Jacobsen for helpful collaborations in the lab. Lastly, I'd like to thank all future generations of graduate students in the Hinderliter lab for their continued interest in and dedication to answering synaptotagmin research questions. I look forward to what's uncovered.

This material is based upon work supported by the National Science Foundation under Grant Number (MCB-0845676). Any opinions, findings, and conclusions or recommendations expressed in this material are those of the authors and do not necessarily reflect the views of the National Science Foundation.

Abstract

Synaptotagmin I (Syt I) is a snaptic vesicle integral membrane protein that has been genetically and biochemically identified as the calcium sensor for synchronous release of neurotransmitter. How Syt I senses a calcium influx and subsequently conveys the information to its numerous binding partners to coordinate neurotransmission has been a question of extensive study for decades; however, an underlying mechanism for this function has yet to be determined. To address this issue, we hypothesized that Syt I's signaling capabilities stem from marginal stability of and intrinsic disorder within its protein structure. Both features can provide great signaling capacity and structure plasticity required for the protein's diverse and responsive functionalities observed in vivo. To test this hypothesis, a combination of differential scanning calorimetry, isothermal titration calorimetry, and fluorescence lifetime spectroscopy were used to determine the stability and binding for Syt I's cytosolic region in buffered solution. First, to test for cooperative signaling between Syt I's tandem C2 domain (C2A and C2B), both domains were thermally denatured separately and tethered together. By comparing the very weak, but additive free energies of these three protein constructs, it was found that the two marginally stable C2 domains cooperatively interact through negative coupling, a destabilizing interaction. Second, to test the potential impact of disorder on Syt I's calcium sensing function, two constructs of the C2A domain (one with the long disordered C2 domain-membrane linker and one without) were thermally denatured and titrated with saturating calcium. The C2A construct with the disordered linker was found to be less stable and bound calcium in a cooperative manner. The C2A construct without the disordered linker was more stable and did not exhibit cooperative binding. Taken together, the above findings support the hypothesis that Syt I's cooperative signaling likely stem from weak energetics. Such a model for protein function suggests Syt I coordinates and integrates its interactions through subtle refinements in its conformational ensemble.

Table of Contents

List of Tables

List of Figures

List of Abbreviations

SNAP-25 – synaptosomal-associated protein 25
Syt I – synaptotagmin I
Ca^{2+} – calcium ion
POPS/PS – phosphatidylserine
PI/PIP2 – phosphatidylinositol bisphosphate
POPC/PC - phosphatidylcholine
SNAREs – soluble NSF attachment protein receptors
DSC – differential scanning calorimetry
FLT – fluorescence lifetime spectroscopy
Trp – tryptophan
EPR – electron paramagnetic resonance
FRET – fluorescent resonance energy transfer
KCl – potassium chloride
MOPS – 3-(N-morpholino)propanesulfonic acid
EGTA – ethylene glycol tetraacetic acid
LUVs – large unilamellar vesicles
BAPTA – (1,2-bis(*o*-aminophenoxy)ethane-N,N,N',N'-tetraacetic acid)
MBP – maltose binding protein
PDB – protein database

Chapter 1: Signal Transduction in the Nervous System

1.1 – The Physiological Context

Signals are sent throughout the human body via the nervous system. The nervous system is a specialized network of cells optimally positioned to send and receive messages to and from all parts of the body. The nervous system innervates muscle, endocrine glands, sensory systems, and other tissues as a way of influencing and maintaining the homeostatic collaboration of all organ systems. On a microscopic level, this elaborate integrative network largely consists of nerves. Nerves are conduits for tens to hundreds of neurons, the fundamental cellular unit of the nervous system. Just like the over arcing function of the nervous system, the neuron structure has the same general form for its signaling function: dendrites for receiving incoming information; a cell body for integrating all information received; an axon for sending the integrated message onward; and an axon terminal for delivering the message to the target tissue[1].

Neurons use a combination of electrical and chemical signals to convey information. When a neuron receives incoming information from the extracellular environment, action potentials are stimulated. The action potential is generated by the concerted opening and closing of sodium and potassium ion channels. The local difference in membrane potential that results is subsequently propagated down the axon. Once the action potential reaches its terminal, it triggers the opening of voltage-gated calcium ion channels. The resulting influx of calcium triggers fusion of neurotransmitter-containing vesicles with the plasma membrane simultaneously releasing neurotransmitter into the synaptic cleft and converting an electrical signal into a chemical signal[1].

1.2 – The Molecular Context

The release of neurotransmitter that results from action potential-induced influx of calcium is a process that requires multiple protein and lipid mediators (Figure 1.1). Some of the key proteins include synaptobrevin, SNAP-25, and synataxin 1, which collectively constitute the SNARE complex (a super helical structure thought to zipper together and bring adjacent membranes in close proximity), complexin (a regulatory protein that binds the SNARE complex and is thought to halt docked vesicles and prevent fusion events from occurring), and several others [2]. Some of the key lipid mediators include phosphatidylserine, phosphatidylethanolamine, phosphatidylinositol, and cholesterol, each of which contributes to the fusion event either directly through lipid packing tendency or indirectly by tuning the function of membrane-associated proteins. At the center of these molecular mediators is the vesicle-localized protein synaptotagmin I, the protein responsible for sensing calcium and synchronizing release of neurotransmitter.

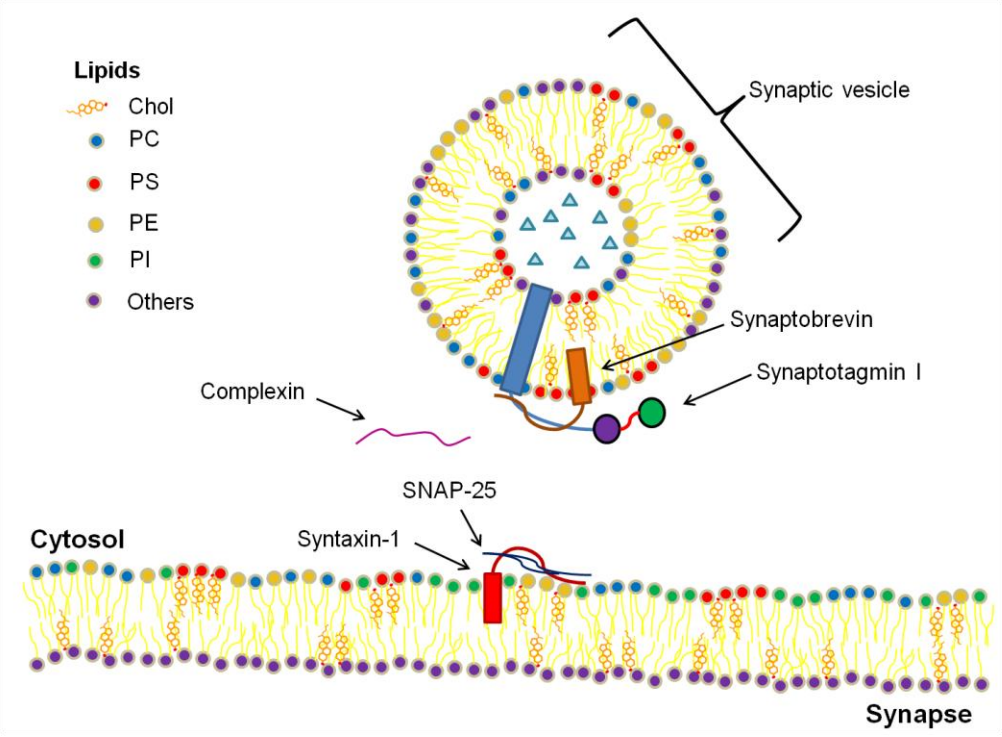

Figure 1.1 A simplified diagram representing the distribution of key lipids and proteins involved in regulated fusion of synaptic and plasma membranes. The above diagram shows a few key players that mediate release of neurotransmitter. The blue triangles within the synaptic vesicle are meant to represent neurotransmitter. The true number of protein and lipid species present are considerably larger [3].

1.2.1 – Synaptotagmin as a mediator of neurotransmission

Synaptotagmin was first identified as a probable calcium sensor for the synchronous release of neurotransmitter through genetic knock-out experimentation; an absent, truncated, or otherwise aberrant form of synaptotagmin was found to severely alter synchronous neurotransmitter release and often resulted in death of the host organism shortly after birth [4-6]. After these initial genetic studies, intense biochemical investigation of synaptotagmin I (the main isoform found in neurons) ensued. While these studies revealed much in the way of ligands, binding partners, and fusion kinetics, the fundamental properties that imparted synaptotagmin I with the ability to sensitively detect calcium and subsequently convey that information to all its binding partners have remained elusive[7].

1.2.2 – Redefining neuronal calcium sensing of synaptotagmin I

The term "calcium sensor," in a neuronal context, refers to a way of coupling a transient and subtle change in second messenger to the efficient release of neurotransmitter. While the concept seems simple, how a protein can accomplish such a task is not entirely clear. However, when considering the context of the protein,

predictions can be made. Calcium is a signal for many events in any cell. As such, the intracellular concentration of calcium ion is tightly regulated and generally quite low [8-10]. Because of this, one prediction is that a protein responsible for sensing calcium's presence would likely employ cooperativity as a functional mechanism; the increasingly favorable binding of each additional cation would ensure adequate chelation of fleeting calcium. Because calcium binding to synaptotagmin I is the trigger for synchronous neurotransmitter release[11], the next question is how could the protein transduce the chelation signal to the rest of the exocytotic machinery? One possibility is marginal stability. In thermodynamic models of multi-domain proteins, like synaptotagmin, there appears to be an inverse correlation between allosteric coupling and stability[12]. Such a relationship could provide a means for propagating calcium ligation to distant sites that interact with other binding partners. Moreover, because since synaptotagmin interfaces with proteins of differing structure and spatial orientation as well as two dynamic membrane leaflets, a weakly held together protein would be better suited for accommodating such a wide array interactions.

In the chapters that follow, the above definition is developed through the combined use of calorimetry and fluorescence. Not only are the isolated domains of synaptotagmin I weakly held together, but their signaling capacity increases when tethered together due to a destabilizing interaction (Chapter 2). Such a finding provides great potential for conformational plasticity and signaling (Chapter 3). Indeed, when the latter was explored using one isolated domain, a disorder-induced weakening was found to tune the protein's sensitivity to calcium (Chapter 4). Collectively, this body of work

provides a new mechanistic basis for synaptotgamin's signaling capability and functional plasticity.

Chapter 2: Negative Coupling as a Mechanism for Signal Propagation between C2 Domains of Synaptotagmin I*

2.1 – Introduction

Regulated exocytosis of neurotransmitter requires the fusion of synaptic vesicles with the plasma membrane of the presynaptic neuron. This complex process is mediated by several key proteins including synaptobrevin, syntaxin-1, SNAP-25, complexins, and synaptotagmin I[13-17]. Synaptotagmin I (Syt I), a synaptic vesicle integral membrane protein, has been implicated in sensing the calcium (Ca^{2+}) influx that ultimately triggers fusion between vesicle and plasma membranes[5,11,18]. Syt I consists of a short luminal N-terminus, a transmembrane region, and two cytosolic C2 domains in tandem known as C2A and C2B. Both domains bind Ca^{2+} and acidic phospholipids that modulate fusion[19-23] such as phosphatidylserine (PS) and phosphatidylinositol (PIP_2). In addition to binding Ca^{2+} and lipid, Syt I also interacts with several proteins involved in vesicle fusion, including members of the SNARE complex[24-27].

How Syt I utilizes two C2 domains to rapidly transmute binding information from Ca^{2+} and lipid ligands as well as from proteins within its immediate vicinity to facilitate fusion between vesicle and plasma membranes is not well understood, with conflicting evidence both for and against domain cooperation[20,25,28-32]. It has been suggested that the function of tandem lipid-binding domains may be one of coincidence detection[33]. In this framework, the differential binding preferences of each domain allow for appropriate temporal and spatial positioning of the protein and, in the case of Syt I, additional

* Note: This chapter was reproduced in its entirety under the terms of the Creative Commons Attribution License from the following open-access article: Fealey ME, Gauer JW, Kempka SC, Miller K, Nayak K, et al (2012) Negative Coupling as a Mechanism for Signal Propagation between C2 Domains of Synaptotagmin I. PLoS ONE 7(10):e46748

components needed for fusion. This mechanistic view as it applies to C2 domains implies that tethering C2A to C2B would result in their additive, independent function.

Recent theoretical studies[12,34] provide an alternative, cooperative function for two domain signaling proteins. Briefly, to both detect a signal (which relies on redistributing domain conformations or conformers[35]) and propagate it, the protein needs to have a unique set of domain stabilities and a free energy of interaction (Δg_{int}) that collectively facilitate coupling. The sign of Δg_{int} describes the nature of the inter-domain coupling and how the domains communicate with one another. In positive coupling, both domains will experience a similar stabilizing effect upon introducing a perturbation. With negative coupling, the two domains experience opposite stabilizing effects. If, for instance, the perturbation is ligand binding and Δg_{int} is positive, both domains will experience a stabilizing effect. Regardless of Δg_{int} sign, introducing a perturbation that changes the conformer distribution (also known as an ensemble) of one domain will directly impact the ensemble of the adjacent domain.

In light of the theoretical studies cited above, we propose that rather than having an additive coincidence detector function, the C2 domains of Syt I cooperatively propagate binding information through inter-domain coupling. This type of interaction would be of functional significance as each domain would become an allosteric regulator of the other. Ligand binding to C2B, for instance, would not only redistribute C2B's ensemble, but would also increase or decrease the probability of binding-competent conformers of C2A being occupied.

Testing for the proposed interaction and quantifying its energetic value is difficult because of Δg_{int}'s necessarily small magnitude. This problem is best appreciated within

the context of the C2 domain's restricted volume. The nine residue linker that tethers C2A and C2B together (Fig. 2.1A) significantly reduces accessible solution volume, causing the local concentration of each domain to increase well beyond attainable solution concentrations (Fig. 2.1B). Consequently, there is an increased probability of domain association. If Δg_{int} were large relative to the two domains in this context, then C2A and C2B would predominantly be in an associated state; this arrangement could greatly reduce the conformational freedom of the individual domains and negatively impact the signaling capacity of the protein. To preserve this function, Δg_{int} would need to be small.

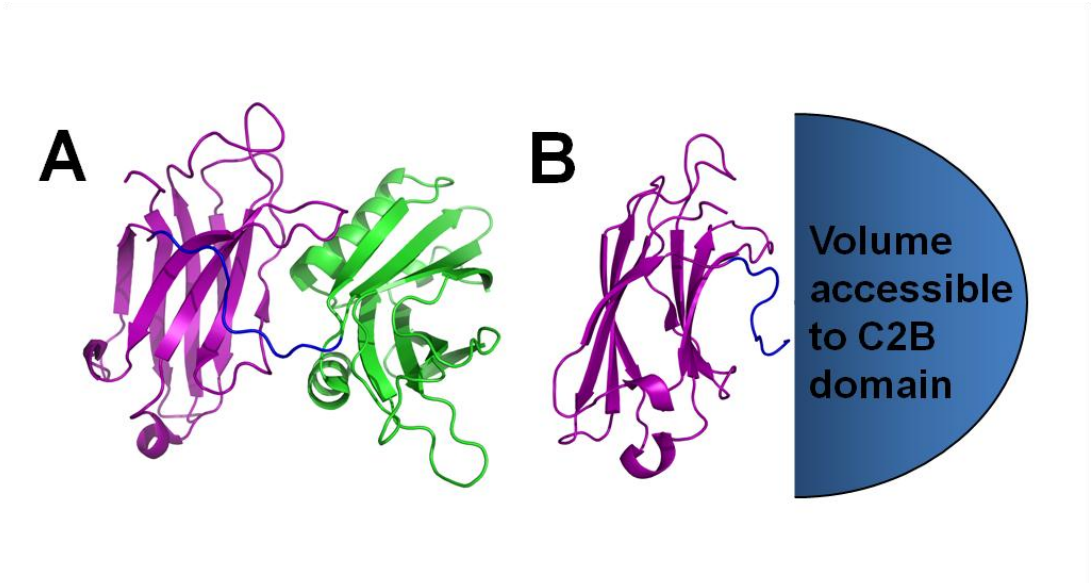

Figure 2.1 Restricted volume effect of domain tethering. (A) Crystal structure of Syt I in the absence of ligand (PDB 2R83). The C2A domain, nine-residue linker region, and C2B domain are colored purple, blue, and green, respectively. (B) Conceptual representation and illustrative calculation of the volume accessible to the C2B domain with respect to C2A. Because the C2B domain is tethered to C2A, the volume it can occupy is restricted. This significantly increases the local concentration of C2B. If, for

instance, the volume is calculated using the length of the linker and width of C2B as an approximate hemisphere radius (Pymol measurement of roughly 57 Å), the accessible volume is $4x10^{-19}$ cm^3. Assuming 1 molecule of C2B occupies this volume, its local concentration is equal to (1 molecule C2B/$6.022x10^{23}$ molecules per mole)/($4x10^{-25}$ m^3) or ~4 M. The local concentration of the C2A domain can be approximated in an analogous way. The resulting concentrations would shift the association equilibrium in the direction of a bound state.

Since our hypothesis is based upon subtle differences in protein energetics, two highly sensitive methods were employed to test it, namely differential scanning calorimetry (DSC)[36-37] and fluorescence lifetime spectroscopy (FLT)[35], the latter of which selectively monitors tryptophan residue fluorescence. Constructs of C2A, C2B, and C2AB (containing just the cytosolic C2 domains) were thermally denatured using each technique. The resulting DSC and FLT data sets were analyzed by globally fitting both to a two-state model of protein unfolding (see Text S1). The fit parameters of enthalpy change (ΔH_{Tm}), heat capacity change (ΔC_p), and melting temperature (T_m) were then used to determine free energies of stability at physiological temperature ($\Delta G°_{37°C}$) using the Gibbs-Helmholtz equation (equation (5)). The validity of the two-state model was judged by comparison of experimental (ΔH_{cal}) and calculated (ΔH_{Tm}) enthalpies. By comparing the additive free energies of the individual C2 domains with the C2AB construct, we were able to identify a negative coupling interaction between the C2 domains of Syt I. The quantitative description of this interaction provides a mechanistic means by which Syt I cooperatively propagates binding information throughout both

domains and may represent a capacity for coordinating the molecular events of neurotransmitter release.

2.2 – Materials and Methods

2.2.1 – Materials

Potassium chloride (KCl) was Puriss-grade. Calcium chloride dihydrate, 3-(N-morpholino) propanesulfonic acid (MOPS), and ethylene glycol-bis(2-aminoethyl)-N,N,N',N'tetra-acetic acid (EGTA) were all Biochemika grade from Fluka Chemical Corp. All buffers were decalcified using Chelex-100 ion-exchange resin (Bio-Rad Labs). All lipids including 1-palmitoyl-2-oleoyl-*sn*-glycero-3-phosphocholine (POPC, 16:0,18:1PC), 1-palmitoyl-2-oleoyl-*sn*-glycero-3-phosphoserine (POPS, 16:0,18:1PS), and 1-stearoyl-2-arachidonoyl-*sn*-glycero-3-phospho-(1'-myo-inositol-4',5'-bisphosphate) (PIP_2, 18:0,20:4PI(4,5)P_2) were obtained from Avanti Polar Lipids (Birmingham, AL).

2.2.2 – Protein Purification

Human Syt I C2A and C2AB constructs were purified as previously described[35,38]. Human Syt I C2B was expressed and purified as a maltose-binding fusion protein. Full details of this domain's purification can be found in the supporting material (Fig. 2.3). Final protein concentrations prior to use in denaturation scans were determined using a Nanodrop (ThermoScientific) with each construct's respective A280 extinction coefficient.

2.2.3 – Preparation of Lipid Vesicles

Large unilamellar vesicles (LUVs) consisting of POPC:POPS (60:40) and POPC:PIP_2 (95:5) were prepared as previously described[35]. PIP_2-containing vesicles were

not, however, lyophilized. Concentrations for all lipid stock solutions were verified using a phosphate assay[39].

2.2.4 – DSC

DSC experiments were performed on a NanoDSC (TA Instruments, New Castle, DE) at a scan rate of 1 °C/min. To see if measured enthalpies varied with concentration or scan rate, all constructs were denatured over a range of concentrations and scan rates[35]. In C2A + C2B DSC control scans, concentrations of each domain were equimolar. All scans were conducted in chelexed 20 mM MOPS, 100 mM KCl, pH 7.5. Scans performed in the absence of Ca^{2+} contained 500 µM EGTA. Scans of both C2A and C2B domains in the presence of Ca^{2+} had ligand concentrations sufficient for >95% saturation of Ca^{2+}-binding sites (binding constants obtained from both binding studies[40] with terbium ion and from isothermal titration calorimetry studies). For the C2AB construct, a Ca^{2+} concentration of 5.2 mM was used. The concentration of Ca^{2+} stock solution used for all scans was verified using both a calcium ion selective electrode (ThermoScientific) and a BAPTA chelating assay (Invitrogen/Molecular Probes, Eugene, OR). Scans carried out with lipid contained LUVs composed of either a 60:40 mixture of POPC:POPS or a 95:5 mixture of POPC:PIP_2. Excess ligand was intentionally used to thermodynamically characterize a specific subset of conformers (only conformers that bind Ca^{2+}, for instance) and not a heterogeneous population of conformations (a mixture of ligand-bound and unbound Syt I). To apply reversible thermodynamics, some evidence of reversible protein folding is needed. By comparing the measured enthalpies of the first and second scans of a single DSC sample, a percent reversibility was determined.

2.2.5 – FLT

FLT experiments were performed on a Lifetime Spectrometer (Fluorescence Innovations, Bozeman, MT) using nanomolar protein concentrations. Under some ligand conditions, higher concentrations were needed to obtain good signal. Scans were conducted in chelexed 20 mM MOPS, 100 mM KCl, pH 7.5. No time-resolved measurements were made. Instead, the integrated intensity of the lifetime decay was used to selectively monitor intrinsic fluorescence of endogenous tryptophan residues (excitation and emission wavelengths of 295 and 340 nm, respectively). Change in fluorescence emission for each construct was monitored as a function of increasing 2 °C temperature increments. In scans free of Ca^{2+}, 500 μM EGTA was added as background. In scans with Ca^{2+}, both C2A and C2B binding sites were >95% saturated (as described above in DSC section). For C2AB, a Ca^{2+} concentration of 5.1 mM was used. The same Ca^{2+} stock solution described above was used for FLT samples. Scans with lipid contained LUVs of identical composition as described above for DSC. Percent reversibility was measured by comparing the integrated fluorescence lifetime intensity of the sample before heating and after cooling. All data sets were analyzed at an emission wavelength of 345 nm to verify absence of contributing water fluorescence at 340 nm. The fluorescence signal measured was normalized to the calculated intensities from the two-state model and subsequently displayed as "Normalized Intensity" in each corresponding plot.

2.2.6 – Global DSC and FLT Analysis

The free energy of stability for each construct under each set of ligand conditions was determined by globally fitting denaturation data from DSC and FLT methods to a two-state transition model. For full details of this model and its application, see supporting materials. In this model, there is equilibrium between native (N) and denatured (D) states, represented by the equilibrium constant below:

$$K = [D]/[N] \quad (1)$$

The equilibrium constant can be used to represent fractions of folded (f_N) and unfolded (f_D) protein throughout the transition. As a protein undergoes thermal denaturation in the DSC, the heat capacity ($C_p(T)$) of the sample cell changes as the fraction of unfolded protein changes:

$$C_p(T) = f_D \, \Delta H(T) \, d/dT \quad (2)$$

Where $\Delta H(T)$ is the associated enthalpy. When the protein is denatured in FLT, the tryptophan residues become more solvent exposed and lose much of their initial intensity. Throughout the unfolding transition, the total fluorescence signal measured (S(T)) is a composite of native (S_N) and denatured (S_D) protein fluorescence and depends on the fraction of each present at a given temperature:

$$S(T) = (S_N\text{-}S_D)/(K + 1) + S_D \quad (3)$$

Where S_N and S_D are approximated by using linear equations. By substituting the Gibbs-Helmholtz equation (equation (4)) into equation (3) and equation (2) above and making simple rearrangements, data from both methods were fit simultaneously using a non-linear least squares regression approach (see supporting materials)[41].

$$\Delta G° = \Delta H_{Tm}(1 - T/T_m) + \Delta C_p(T - T_m - T(\ln(T/T_m))) \quad (4)$$

The terms ΔH_{Tm}, T_m, and ΔC_p are the fit parameters in this model, however, to further constrain this fit, ΔC_p was fixed using an empirical approximation method that showed good agreement with experimentally-derived values[42]. The fixed ΔC_p values for C2A, C2B, and C2AB were 1.92, 2.19, and 4.53 kcal/mole, respectively. The parameters resulting from the global fit were subsequently substituted into equation (4) to determine the free energy of stability at any specified temperature (T) which in this study was the physiological temperature of 37 °C. Four replicates of each technique (for a total of $n = 8$, when achievable) were used in the global fit for each set of conditions. Each data point within each technique is the average of the 4 replicates with the associated error plotted as 95% confidence interval. The error associated with fit parameters and the model line, which represents the global fit for all 8 data sets, were determined using the SolverAid function of Excel as described by De Levie[43].

The entropy change associated with the unfolding transition (ΔS) was calculated using the $\Delta G°_{37°C}$, ΔH_{Tm}, and the physiological temperature of 310 K of each protein construct under each set of ligand conditions using the Gibbs free energy equation:

$$\Delta G° = \Delta H - T\Delta S \qquad (5)$$

2.3 – Supporting Material

2.3.1 – Two-State Model of Protein Unfolding

In the two-state model of protein unfolding, a conformationally flexible protein exists in either a native (N) or denatured (D) ensemble, wherein conformers of each ensemble have similar energies. These two ensemble states are represented by an equilibrium constant:

$$K = [D]/[N] \tag{S1}$$

The equilibrium constant is directly related to free energy of stability ($\Delta G°$, Eq. S2 and Eq. S3). The equilibrium constant is not easily measured directly in the laboratory. Instead, free energy is approached from a calorimetric direction. Free energy has enthalpic ($\Delta H(T)$) and entropic ($\Delta S(T)$) contributions, both of which are temperature dependent functions:

$$\Delta G° = -RT\ln(K) \tag{S2}$$

$$\Delta G° = \Delta H(T) - T\Delta S(T) \tag{S3}$$

$$\Delta H(T) = \Delta H_{Tm} + \int_{Tm}^{T} \Delta C_p(T)\, dT \tag{S4}$$

$$\Delta S(T) = \Delta H_{Tm}/T_m + \int_{Tm}^{T} \Delta C_p(T)\, d\ln(T) \tag{S5}$$

Where ΔH_{Tm} is a reference enthalpy typically obtained from a calorimeter, T_m is a reference temperature (typically the melting temperature of the protein), and $\Delta C_p(T)$ is the difference in sample cell heat capacity between the native and denatured ensemble states. If $\Delta C_p(T)$ is assumed to be temperature independent (designated by the notation ΔC_p), Eq. S4 and Eq. S5 can be substituted into Eq. S3 to obtain the Gibbs-Helmholtz equation:

$$\Delta G° = \Delta H_{Tm}(1 - T/T_m) + \Delta C_p[T - T_m - T(\ln(T/T_m))] \tag{S6}$$

Eq. S6 enables calculation of protein stability at any temperature (T).

At any point in the unfolding transition, the fraction of native (f_N) and denatured (f_D) protein can be determined using mass balance for total protein (P_T) and the equilibrium constant:

$$P_T = [D] + [N] \quad \text{(S7)}$$

$$f_N = [N]/P_T = [N]/([D] + [N]) = 1/(K + 1) \quad \text{(S8)}$$

$$f_D = [D]/P_T = [D]/([D] + [N]) = K/(K + 1) \quad \text{(S9)}$$

As a protein thermally denatures in a differential scanning calorimeter (DSC), the heat capacity ($C_p(T)$) of the sample cell changes as the fraction of unfolded protein changes:

$$C_p(T) = f_D \, \Delta H(T) \, d/dT \quad \text{(S10)}$$

Application of the Product Rule expands the above derivative into two terms:

$$C_p(T) = (f_D(d/dT))\Delta H(T) + f_D(\Delta H(T)(d/dT)) \quad \text{(S11)}$$

Differentiating Eq. S4, assuming $\Delta C_p(T)$ is a temperature-independent function, simplifies the expression to ΔC_p. Differentiating f_D requires further use of the Quotient Rule and substitution of nested temperature-dependent functions (Eq. S2 and Eq. S6 into Eq. S9):

$$f_D \, (d/dT) = (e^{-(\Delta HTm(1 - T/Tm) + \Delta Cp[T - Tm - T(\ln(T/Tm))])} / e^{-(\Delta HTm(1 - T/Tm) + \Delta Cp[T - Tm - T(\ln(T/Tm))])} + 1) \, d/dT \quad \text{(S12)}$$

$$f_D \, (d/dT) = [((\Delta H_{Tm}/T - \Delta C_p T_m/T + \Delta C_p)/RT)((K(K + 1)) - (K^2/RT))]/((K+1)^2) \quad \text{(S13)}$$

Substituting Eq. S13 back into Eq. S11 generates the two-state model used to fit DSC data:

$$C_p(T) = \Delta H(T)([((\Delta H_{Tm}/T - \Delta C_p T_m/T + \Delta C_p)/RT)((K(K + 1)) - (K^2/RT))]/$$
$$((K+1)^2)) + (\Delta C_p K/(K + 1)) + FBL_{DSC} \quad (S14)$$

Where FBL_{DSC} refers to the folded baseline heat capacity determined with a linear equation.

To obtain a more stringent and complete fit, denaturation data from FLT was simultaneously fit to the same model. FLT selectively monitors intrinsic fluorescence of tryptophan residues (Trp) in a protein. In the native state, the environment surrounding Trp allows for maximum fluorescence. When the protein denatures, the Trp become solvent exposed and lose much of their initial intensity. Throughout the transition, the total signal measured (S(T)) is a composite of native (S_N) and denatured (S_D) protein fluorescence:

$$S(T) = S_N + S_D \quad (S15)$$

The contribution from both native and denatured states depends on the fraction of each present at a given temperature. The total integrated fluorescence lifetime signal can be expressed as such:

$$S(T) = (S_N\text{-}S_D)/(K + 1) + S_D \quad (S16)$$

S_N and S_D are determined with linear functions before (the folded baseline, FBL_{FLT}) and after (the unfolded baseline, UBL) the unfolding transition:

$$S_N = FBL_{FLT} = (m_N)T + int_N \quad (S17)$$

$$S_D = UBL = (m_D)T + int_D \quad (S18)$$

Where m and int are the slope and intercept, respectively, for each baseline. To determine S_N throughout the course of the denaturation, the signal contributed by S_D must be

subtracted off the measured composite signal. The model for FLT signal as a function of temperature becomes:

$$S(T) = (FBL_{FLT} - UBL)/(K + 1) + (UBL) \quad \text{(S19)}$$

By substituting a rearranged Eq. S2 and Eq. S6 into Eq. S19, the fitting of FLT and DSC denaturation data are linked and can be subject to non-linear least squares regression.

2.3.2 – Fluctuation Dissipation Theorem

The fluctuation dissipation theorem describes fluctuations about a mean for a given system. In the case of protein denaturation where heat capacity (C_p) is measured, the enthalpy fluctuates and the theorem is[44]:

$$C_p = (H^2 - \langle H \rangle^2)/RT^2 \quad \text{(S20)}$$

Where H is enthalpy in a Gaussian distribution about the mean $\langle H \rangle$, R is the gas constant, and T is temperature. C_p is thus proportional to the enthalpy deviation ($H^2 - \langle H \rangle^2$) of either folded or unfolded states of a protein. The heat capacities for native and denatured states differ due to the extent of hydrophobic residue exposure in aqueous solution. As such, the native $H^2 - \langle H \rangle^2$ is much smaller than the denatured $H^2 - \langle H \rangle^2$. Using the folded and unfolded heat capacity baselines obtained from the DSC, the relative widths of the folded and unfolded enthalpy distributions can be approximated.

The distance between the mean enthalpies of each distribution is directly measured by the calorimeter and is the change in enthalpy (ΔH) between folded and unfolded states of the protein. By combining estimates for folded C_p and unfolded C_p with the change in enthalpy, enthalpy distribution plots can be sketched (Fig. 2.2). The

assembly of these plots allows for qualitative monitoring of ligand-induced changes in the protein's native and denatured enthalpy distributions.

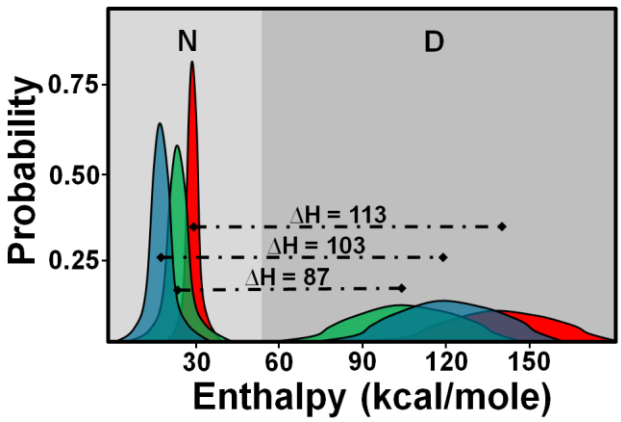

Figure 2.2 Illustration of the fluctuation-dissipation theorem applied to C2AB. Native (N) and denatured (D) fluctuation distributions for C2AB in the absence of any ligand (blue), in the presence of POPC:POPS (60:40) liposomes (green), and in the presence of Ca^{2+} (red). Note that the energetic distributions of an N/D pair become closer together or farther apart depending on the type of ligand.

2.3.3 – Purification of Isolated C2B Domain

The C2B purification was similar to C2A and C2AB with respect to plasmid preparation, *E. coli* transformation and growth, cell lysis, and nucleic acid degradation. However, C2B was expressed with a 6xHis-tagged maltose-binding protein (MBP). The amino acids linking C2B to MBP formed a cleavage site for a 6xHis-tagged tobacco etch virus (TEV) protease. After overnight treatment with benzonuclease at 4 °C, C2B-MBP fusion protein was equilibrated with slurried Ni-NTA agarose media (Qiagen) in 20 mM MOPS/100 mM KCl/10 mM imidazole/pH 7.5 buffer for 3 hours at 4 °C. The 10 mM imidazole prevented non-specific protein binding. After equilibration, the slurried media

was transferred into a column. Complete elution of undesired protein was monitored by measuring the A280 using a Nanodrop (Thermo Scientific). To remove nucleic acid, a 10 column volume wash was carried out with 20 mM MOPS/1M KCl/pH 7.5 buffer. The column was re-equilibrated with the 10 mM imidazole buffer. The nucleic acid-free fusion protein (A260/A280<0.8) was then eluted with 20 mM MOPS/100 mM KCl/250 mM imidazole/pH 7.5 buffer. Eluted MBP-C2B was dialyzed with TEV protease in 20 mM MOPS/100 mM KCl/pH of 7.5 buffer (3 mg of TEV protease were added for every 150 mg of fusion protein). After >14 hours, cut MBP-C2B and TEV protease were passed over the column. C2B was collected in pass through and its purity was assessed with the Nanodrop (A260/A280<0.8) and gel electrophoresis (Fig. 2.3). Pure C2B was dialyzed in chelexed Fluka grade 20 mM MOPS/100 mM KCl/pH 7.5 buffer prior to use in denaturation studies. Concentrations were determined using an A280 extinction coefficient of 19060 cm^{-1} M^{-1}.

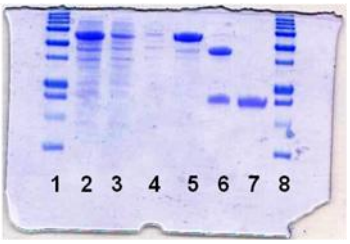

Figure 2.3 Effectiveness of the C2B purification protocol used for this study. Prominent band in lanes 2, 3, and 5 are MBP-C2B after cell lysis (2), during elution of unwanted protein (3), and during 250 mM imidazole elution (5). Lane 6 shows separation of MBP from C2B. Lane 7 shows pure C2B after passing cut MBP-C2B over column. Ladder (lanes 1 and 8, Precision Plus, Bio-Rad Labs) has molecular weights (kDa) of 10, 15, 20, 25, 37, 50, 75, 100, 150, and 250.

2.3.4 – Non-Linear Least Squares Regression Analysis

The non-linear least squares regression analysis is a fitting method that matches the output of Eq. S14 and Eq. S19 to the experimental data by manipulating fit parameters (ΔH_{Tm}, ΔC_p, T_m, m_N, int_N, m_D, int_D) within the model equations. The close fit is accomplished in Excel through use of the Solver, which minimizes the total sum of the square differences (Σ(experimental signal – model signal)^2) to fit the data. Error associated with the resulting fit can then be determined with the macro-functions SolverAid, which estimates error using 1) the scaling factor by with the fit parameters were changed, 2) the global sum of the square difference (for all 8 data sets) after fitting has occurred, and 3) the model's numerical outputs for signal (the theoretical heat capacity or fluorescence signal). For more detail on analysis, see: [41,43].

Human Syt I C2B	
Concentration (mM)	*ΔH_{cal} (kcal/mole)*
0.013	45.9
0.014	37.5
0.012	53.2
0.013	47.3
0.014	43.0
0.013	48.7
0.020	42.1
0.015	45.7
0.021	43.7
0.013	45.2
0.012	46.9
Average ΔH_{cal}	45.4
Standard Deviation	4.0

Table 2.1 Complete list of calorimetric enthalpies used to assess concentration dependence of the C2B domain.

Human Syt I C2AB	
Concentration (mM)	*ΔH_{cal} (kcal/mole)*
0.011	104.7
0.013	96.1
0.013	94.9
0.013	85.2
0.013	99.6
0.013	85.2
0.010	86.7
0.012	87.7
0.013	93.6
0.011	100.4
0.015	89.0
0.019	85.9
0.020	85.6
0.011	86.2
0.015	90.8
0.019	91.8
0.020	93.4
Average ΔH_{cal}	91.6
Standard Deviation	6.0

Table 2.2 Complete list of calorimetric enthalpies used to assess concentration dependence of the C2AB cytosolic fragment.

Protein (Environment)	**ΔH_{Tm} (kcal/mole)**	**$\Delta G°$ at 37 °C (kcal/mole)**	**ΔS (kcal/mole·K)**	**T_m (°C)**	**$\Delta H_{Tm}/\Delta H_{cal}$**
C2B (EGTA)	69.2±0.6	1.73±0.08	0.22±0.01	46.4±0.1	1.44
C2B (Ca^{2+})	81.9±0.5	3.79±0.09	0.25±0.01	59.0±0.1	1.39
C2B (PS)	63.4±0.2	1.16±0.01	0.20±0.01	43.5±0.1	1.61
C2AB (EGTA)	103.1±0.4	2.25±0.01	0.32±0.01	45.6±0.1	1.06
C2AB (Ca^{2+})	112.8±0.5	4.09±0.01	0.34±0.01	59.2±0.1	0.97
C2AB (PS)	86.2±0.3	1.68±0.01	0.27±0.01	44.8±0.1	1.05
*C2AB (PIP_2)**	188±3	4.00±0.60	0.59±0.02	44.4±0.1	NA
*C2AB (Ca^{2+}, PIP_2)**	140±1	5.80±0.04	0.42±0.01	58.0±0.1	NA

Table 2.3 Thermodynamic parameters and associated errors for C2B and C2AB using FLT λ_{em} of 345 nm. Analogous controls were performed for C2A. When FLT integrated fluorescence intensity was normalized and globally fit, there was no substantial

variation in calculated fit parameters. This indicated water fluorescence (water raman at 328 nm) at 340 nm was negligible.

2.4 – Results

2.4.1 – Separate C2 Domains are Weak and Conformationally Flexible

To determine the relative stability of one domain compared to the other and whether the C2 domains of Syt I interact, the thermodynamic parameters of C2A and C2B in isolation were extracted from each domain's thermal denaturation. The enthalpies measured for both C2A and C2B constructs did not show strong dependence on either concentration or scan rate, which is consistent with a system reflecting equilibrium (Tables 2.4 and 2.5, Table 2.1)[35,45]. When comparing the denaturation profiles of C2A and C2B (Fig. 2.4) in the presence and absence of Ca^{2+} and lipid ligands, there are clear differences in domain stability, with C2B being generally less stable (Table 2.6). Relative to proteins of similar size, C2A and C2B have markedly low intrinsic stability[46-47]. The two domains also differ from one another in extent of reversible folding, with C2B being minimally reversible (5-30%) as assessed by FLT (no discernible reversibility was found on any second denaturation scan of a DSC sample) as compared to C2A which exhibits nearly complete reversibility (approximately 60-90% by both FLT and DSC[35]).

If C2A and C2B did not interact with one another when tethered together, the DSC denaturation profile would look similar to the superposition of both individual domain denaturations[34]. Such heat capacity profile controls were generated in both the presence and absence of Ca^{2+} and lipid ligands (Fig. 2.5). Despite extensive overlap of excess heat capacities, variable ΔC_p, and in some instances terminal precipitation and large heat capacities, the two resultant peaks provide a reference denaturation profile to which the individual domains and the C2AB construct can be compared.

Table 2.4 Concentration dependence controls for C2B and C2AB. Note that * indicates enthalpies listed above came from averaging multiple denaturations at each specified concentration. For completeness, the overall range of enthalpies represented within the averaged values is also listed. All measured calorimetric enthalpies for both constructs can, however, be seen in Table 2.4 and Table 2.5.

C2B (Scan Rate, 1 °C/min)		**C2AB (Scan Rate, 1 °C/min)**	
Concentration (mM)	*ΔH_{cal} (kcal/mole)**	*Concentration (mM)*	*ΔH_{cal} (kcal/mole)**
0.012	50.1	0.011	97.1
0.013	46.1	0.012	87.7
0.014	43.1	0.013	92.4
0.015	45.7	0.015	89.0
0.020	42.1	0.019	85.9
0.021	43.7	0.020	85.6
Average ΔH_{cal} (kcal/mole)	*Standard Deviation*	*Average ΔH_{cal} (kcal/mole)*	*Standard Deviation*
45.1	2.9	89.6	4.4
ΔH_{cal} Range (kcal/mole)		*ΔH_{cal} Range (kcal/mole)*	
37.5 – 53.2		85.2 – 104.7	

Table 2.5 Scan rate dependence controls for C2B and C2AB. In both cases, measured calorimetric enthalpies for both C2B and C2AB constructs did not strongly depend on scan rate. Analogous controls were performed for the C2A construct in a separate publication.

C2B (Concentration 15 µM)		**C2AB (Concentration 15 µM)**	
Scan Rate (°C/min)	*ΔH_{cal} (kcal/mole)*	*Scan Rate (°C/min)*	*ΔH_{cal} (kcal/mole)*
1.00	42.1	1.00	89.0
1.10	45.7	1.10	86.4
1.15	52.5	1.15	90.8
1.20	49.9	1.20	87.0
Average ΔH_{cal} (kcal/mole)	*Standard Deviation*	*Average ΔH_{cal} (kcal/mole)*	*Standard Deviation*
47.5	4.6	88.3	2.0

Table 2.6 Thermodynamic parameters and their associated error from the global fit of DSC and FLT data.

Protein (Environment)	ΔH_{Tm} (kcal/mole)	$\Delta G°$ at 37 °C (kcal/mole)	ΔS (kcal/mole·K)	T_m (°C)	$\Delta H_{Tm}/\Delta H_{cal}$
C2A (EGTA)	58.7±0.3	2.32±0.05	0.18±0.01	56.0±0.1	0.98
C2A (Ca^{2+})	77.4±0.6	4.23±0.05	0.23±0.01	67.6±0.1	1.08
C2A (PS)	61±1	2.44±0.05	0.19±0.02	55.5±0.2	1.03
C2A (Ca^{2+}, PS)	72.4±0.9	3.73±0.05	0.21±0.01	75.6±0.3	0.86
C2B (EGTA)	69.6±0.6	1.74±0.09	0.22±0.01	46.4±0.1	1.45
C2B (Ca^{2+})	81.8±0.5	3.78±0.10	0.25±0.01	59.0±0.1	1.39
C2B (PS)	63.7±0.1	1.13±0.02	0.20±0.01	43.3±0.1	1.51
C2B (Ca^{2+}, PS)	75.4±0.2	3.41±0.01	0.23±0.01	59.4±0.1	1.92
C2AB (EGTA)	102.9±0.4	2.24±0.01	0.32±0.01	45.6±0.1	1.05
C2AB (Ca^{2+})	112.8±0.5	4.10±0.01	0.34±0.01	59.3±0.1	0.97
C2AB (PS)	86.8±0.4	1.74±0.01	0.27±0.01	45.1±0.1	1.05
*C2AB (PIP_2)**	198±2	4.09±0.45	0.62±0.01	44.2±0.1	NA
C2AB (PIP_2)†	96.0±0.2	2.56±0.01	0.32±0.01	49.0±0.1	1.08
*C2AB (Ca^{2+}, PIP_2)**	136±1	5.53±0.02	0.41±0.01	58.0±0.1	NA

Footnote for Table 2.6: Note that * indicates parameters obtained from fitting just FLT data sets and † indicates parameters obtained from fitting just DSC data sets. EGTA stands for ethylene glycol tetraacetic acid. NA stands for not applicable and is used for instances where just FLT data was fit. As an additional control, FLT signal was collected at 345 nm, normalized, and subsequently globally fit with DSC denaturation data. The thermodynamic parameters that resulted are similar to those presented above, indicating a lack of water fluorescence contribution at the 340 nm wavelength used for this analysis (Table 2.3).

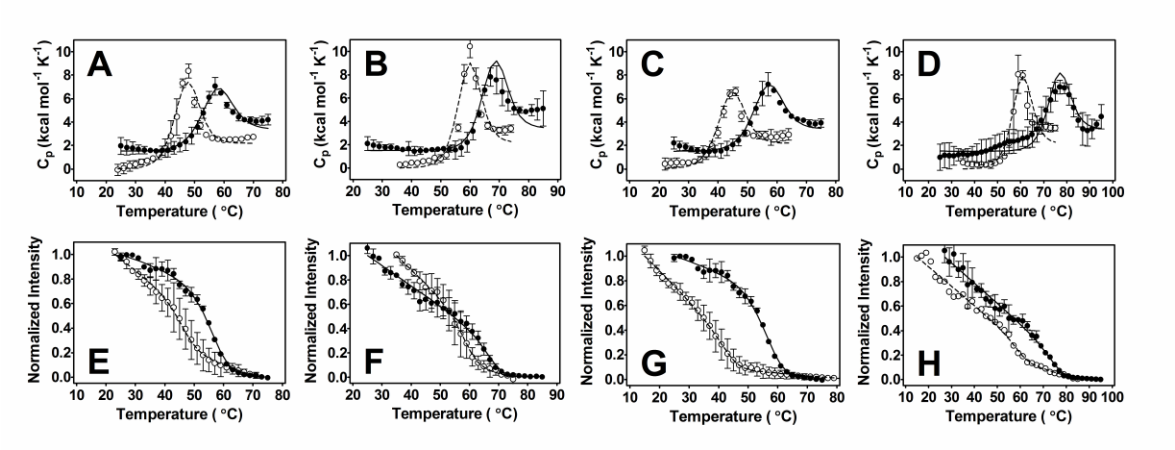

Figure 2.4 Globally-fit denaturation of C2A (●) and C2B (○) using DSC (top) and FLT (bottom) methods. Circles represent the raw data and lines are the fitted model. Higher concentrations refer to DSC samples. (A, E) [C2A] = 13 μM and 0.75 μM, [C2B] = 13 μM and 0.80 μM in the presence of 500 μM EGTA. (B, F) [C2A] = 13 μM and 0.75 μM, [C2B] = 12 μM and 0.75 μM in the presence of Ca^{2+}. [Ca^{2+}] = 800 μM and 770 μM for C2A, [Ca^{2+}] = 5.3 mM and 5.2 mM for C2B. (C, G) [C2A] = 13 μM and 0.75 μM, [C2B] = 15.0 μM and 3.2 μM in the presence of LUVs consisting of 60:40 POPC:POPS. [Lipid] = 870 μM and 50 μM for C2A, [Lipid] = 1.1 mM and 240 μM for C2B. Higher [C2B] in FLT was needed under lipid conditions to better see transition. (D, H) [C2A] = 13 μM and 0.75 μM, [C2B] = 13 μM and 3.2 μM for C2B in the presence of both LUVs and Ca^{2+}. For C2A, [Ca^{2+}] = 800 μM and [lipid] = 870 μM, [Ca^{2+}] = 770 μM and [lipid] = 50 μM. For C2B, [Ca^{2+}] = 5.2 mM and [lipid] = 290 μM, [Ca^{2+}] = 5.2 mM and [lipid] = 70 μM. Low [lipid] for C2B prevented precipitation in calorimeter, but also limited FLT data collection due to flocculation and light scattering [45]. C2A denaturations adapted from Biophysical Journal with permission[35]. C2A denaturation data in isolation was originally used in a former graduate student's thesis, but was include here out of necessity as it is part of answering the research question at hand[48].

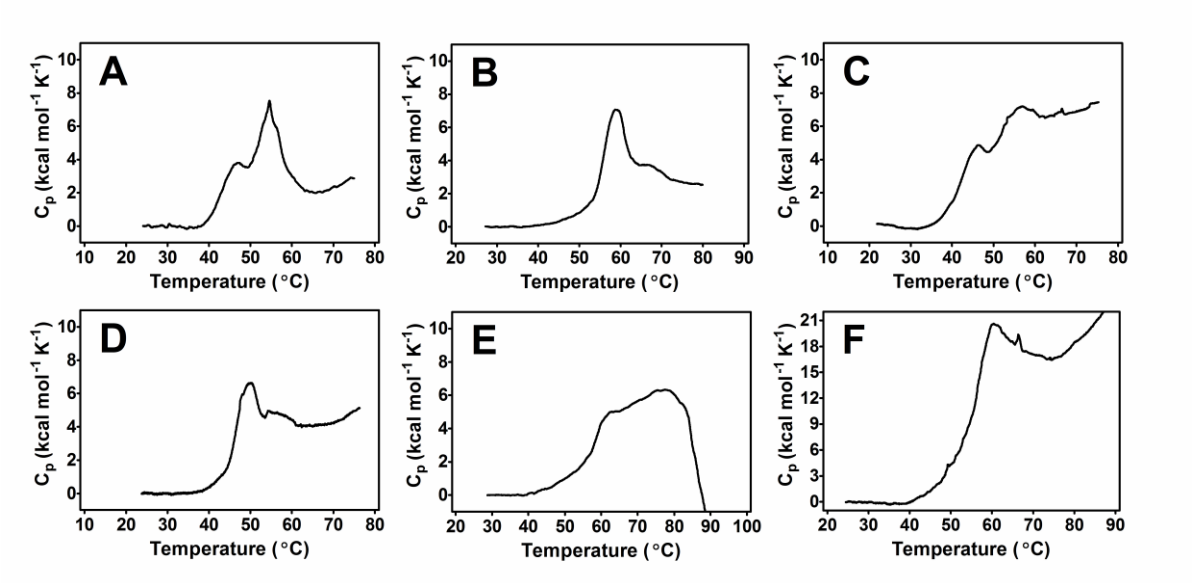

Figure 2.5 Raw DSC data for simultaneous thermal denaturation of separate C2A and C2B domains. (A) 10 μM of each domain in the presence of 500 μM EGTA. (B) 15 μM of each domain in the presence of 5.2 mM Ca^{2+} conditions. (C) 15 μM of each domain in the presence of 2.2 mM PS. (D) 11 μM of each domain in the presence of 2.9 mM PIP_2. (E) 12 μM of each domain in the presence of 1.6 mM PS and 5.2 mM Ca^{2+}. (F) 10 μM of each domain in the presence of 2.8 mM PIP_2 and 5.2 mM Ca^{2+} conditions. Note that in most instances, two separate peaks are seen representing the independent unfolding of each domain. If C2A and C2B within the C2AB construct did not interact, the C2AB denaturation profile would more closely resemble the above heat capacity profiles.

2.4.2– Tethered C2 Domains are Weaker Still and Unfold as One

The Syt I C2AB construct was thermally denatured in the presence and absence of Ca^{2+} and lipid ligands. The enthalpy measured for this construct, like the individual domains, did not show a strong dependence on concentration or scan rate (Tables 2.4 and

2.5, Table 2.2), consistent with a system at equilibrium. In all environments, with the exception of combined Ca^{2+} and lipid ligands, the two domains of C2AB exhibit coupled unfolding (Fig. 2.6). This coupled unfolding is indicative of an inter-domain interaction and contrasts with the model heat capacity profiles of independent domain unfolding depicted in Figure 3. With regard to stability, note again that relative to other proteins of approximately the same size, C2AB is marginally stable (Table 2.6 and Fig. 2.6)[46-47]. Annexin I, for instance, is another Ca^{2+} and membrane binding protein that has an estimated $\Delta G°_{20°C}$ of 11.5 kcal/mol (vs. 2 kcal/mol for C2AB at analogous temperature)[49]. Reversibility as assessed by FLT ranged from 1-24% (no discernible reversibility was seen in any second scan of a DSC sample).

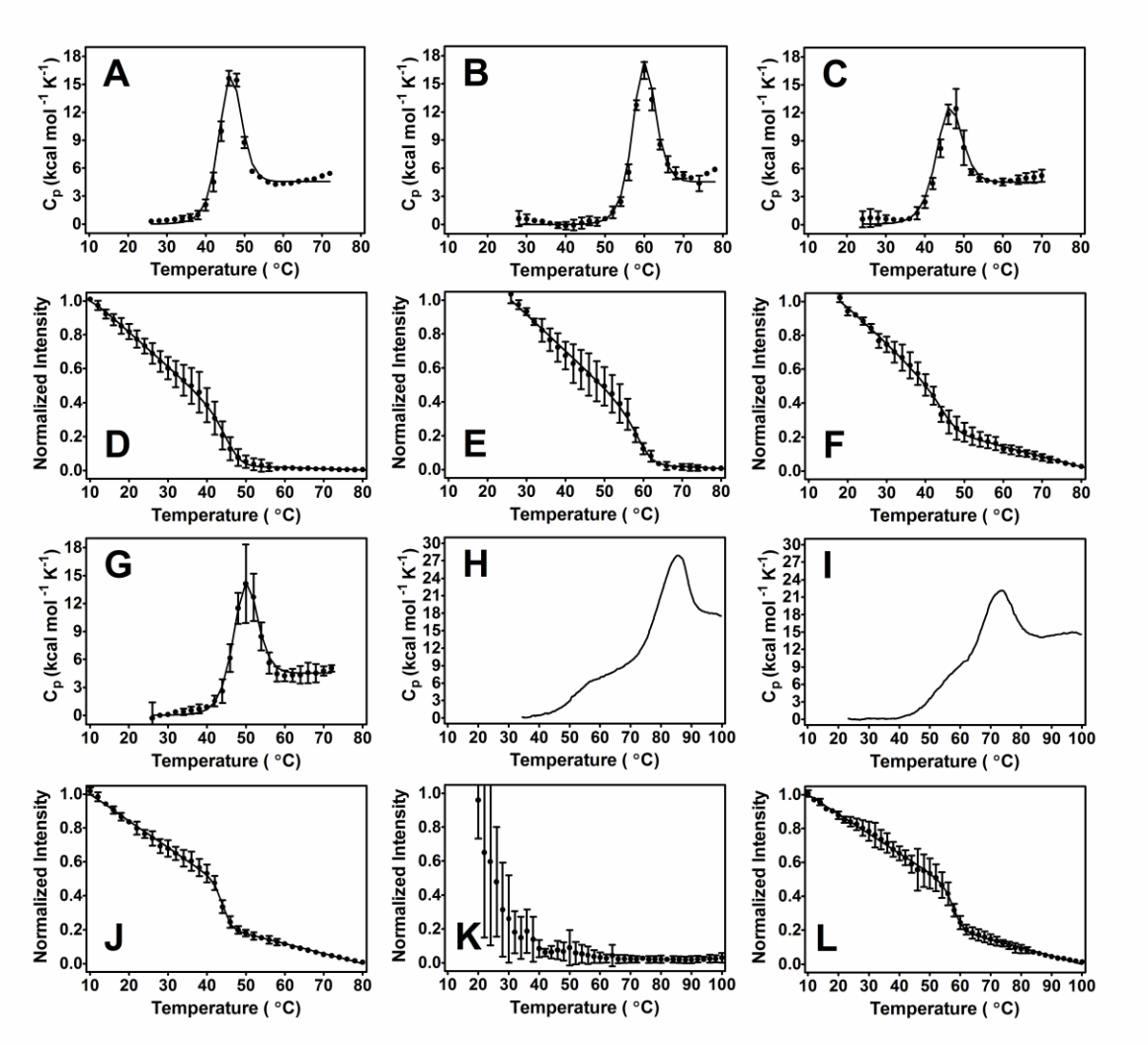

Figure 2.6 Thermal denaturation of C2AB using DSC (A-C, G-I) and FLT (D-F, J-L) methods. Circles represent raw data and lines are the fitted model, excluding panels (H) and (I) wherein the line represents raw heat capacity data. Large and small concentrations refer to DSC and FLT concentrations, respectively. (A, D) 13 μM and 4.5 μM C2AB in the presence of 500 μM EGTA. (B, E) 12 μM and 0.75 μM C2AB in the presence of 5.2 mM and 5.1 mM Ca^{2+}. (C, F) 12 μM and 0.75 μM C2AB in the presence of 1.7 mM and 110 μM PS. (G, J) 11 μM (3 replicates of DSC) and 0.75 μM C2AB in the presence of 2.9 mM and 210 μM PIP_2. (H, K) 12 μM C2AB in the presence of 5.2 mM Ca^{2+} and 1.7 mM PS; 0.75 μM C2AB in the presence of 5.1 mM Ca^{2+} and 110 μM

PS. (F, I) 11 µM (1 replicate of DSC) C2AB in the presence of 5.2 mM Ca^{2+} and 2.9 mM PIP_2; 0.75 µM C2AB in the presence of 5.1 mM Ca^{2+} and 210 µM PIP_2. Both calorimetric denaturations involving PIP_2 had a limited number of replicates due to precipitation. In the absence of any interaction, the two domains would unfold independently. Instead, here the two domains generally unfold as one.

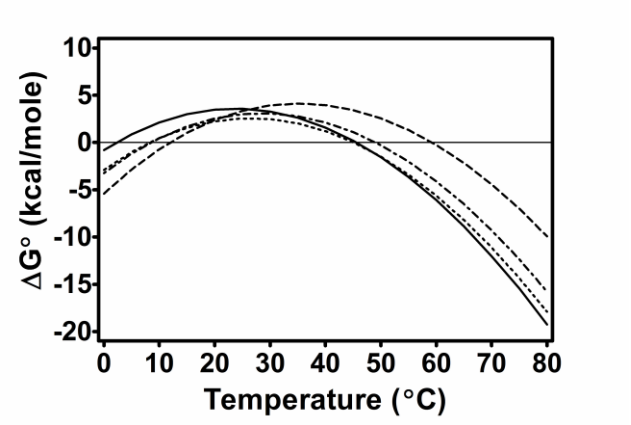

Figure 2.7 Stability of C2AB as a function of temperature in the presence and absence of ligand. Solid, dashed, dotted, and dash-dot-dash lines represent EGTA, Ca^{2+}, phosphatidylserine, and phosphatidylinositol environments. Note that most proteins of comparable size have maxima in the range of 10-20 kcal/mole[46-47].

2.4.3 – C2 Domains Interact through Inverse-Stabilization

When comparing the additive free energies of the isolated C2A and C2B domains with the C2AB construct, a Δg_{int} of -1.8±0.1 kcal/mol was found under ligand-free conditions at 37 °C ($\Delta g_{int} = \Delta G°_{C2AB} - (\Delta G°_{C2A} + \Delta G°_{C2B})$). Since $\Delta g_{int}<0$, the C2 domains of Syt I exhibit a negative inter-domain coupling interaction and the two

domains experience opposite stabilizing effects upon introducing a ligand binding perturbation. This form of coupling is similar to that of other allosteric proteins recently reported[50-51]. Furthermore, when repeating the same calculation for Ca^{2+} and PS conditions, Δg_{int} of -3.9±0.1 kcal/mole and -1.83±0.05 kcal/mole, respectively, were found. This indicates that the magnitude of negative coupling can change in response to ligand, which is in agreement with previous studies[52]. While the magnitude of Δg_{int} can change depending on whether Ca^{2+} or lipid ligands are present, it should be noted that the different combinations of Δg_{int}, $\Delta G°_{C2A}$, and $\Delta G°_{C2B}$ within the tethered construct consistently facilitate domain coupling, though to varying extents.

2.4.4 – Syt I and its Domains are Malleable

The free energies of C2A, C2B, and C2AB in the presence of endogenous ligands were generally higher relative to a ligand-free environment (Table 2.6), with one exception (binding of PS to C2B and C2AB had an overall destabilizing effect). C2AB, for instance, experienced a 0.5 kcal/mole decrease in free energy, nearly 23% of the ligand-free $\Delta G°_{37°C}$ value. This destabilization was more pronounced in C2B where the decrease in free energy was about 35% of the ligand-free $\Delta G°_{37°C}$ value. The phosphatidylinositol lipid PIP_2, in contrast, stabilized C2AB.

The denaturation scans involving PIP_2 differed between DSC and FLT methods (Fig. 2.6G, 2.6I, 2.6J, 2.6L). The C2AB FLT denaturations showed a sharp transition at a lower temperature in comparison to the analogous DSC denaturation. Fitting the two data sets separately generated $\Delta G°_{37°C}$ values of 4.09±0.45 and 2.56±0.01 kcal/mole for FLT and DSC, respectively. Additionally, in C2AB denaturations with PIP_2 and Ca^{2+} ligands,

DSC showed partial peak splitting whereas FLT showed one unfolding transition. The transition measured on FLT was sharp (occurring over a small temperature range) and when fit to a two-state model in isolation generated a $\Delta G°_{37°C}$ of 5.53±0.02 kcal/mole. PS also caused method discrepancy, though only in the presence of Ca^{2+} ligand. When C2AB was denatured using FLT in the presence of PS and Ca^{2+}, no discernible transition could be seen (Fig. 2.6K).

2.5 – Discussion

The purpose of the current study was to test a theory-driven hypothesis in which the C2 domains of Syt I interact to cooperatively disseminate binding information[12]. In isolation, C2A and C2B were found to be energetically distinct. When tethered together with their natural linker, the two domains unfolded as one entity and were found to be less stable together than apart, indicative of a negative inter-domain coupling interaction. These results not only provide further experimental validation[50-54] of recent theoretical work on the thermodynamic basis for domain coupling[12,34], but also a mechanistic means by which the C2 domains of Syt I propagate signal from endogenous ligands throughout both domains of the protein (Fig. 2.8)[55].

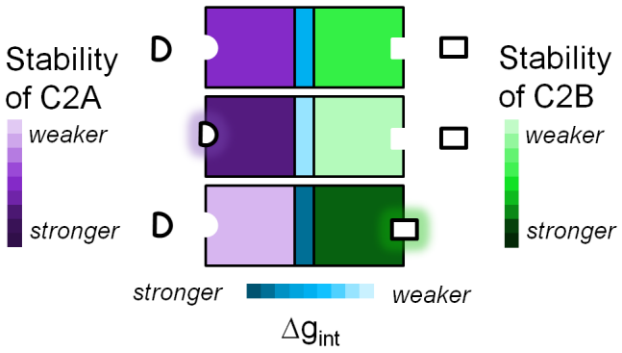

Figure 2.8 Conceptual representation of negative coupling. In the absence of bound ligand (top), domains have basal level stability. When a ligand specific to the C2A domain binds (middle), C2A is stabilized and C2B is destabilized through negative coupling. When a ligand specific to C2B binds (bottom), the opposite effect is seen; C2B is stabilized and C2A is destabilized. Note that binding of domain-specific ligands lowers the probability of binding-competent conformers being occupied in the adjacent domain through domain destabilization, representing a form of allosteric regulation. The extent of

negative coupling, like domain stability, changes depending on the types of ligand present.

Aside from showing negative inter-domain coupling, the results presented here also indicate that the interaction is subject to modulation by Ca^{2+} and phospholipid ligands. The general observation of marginal stability in all three protein constructs relative to proteins of similar size indicates that Syt I has a larger degree of conformational freedom (i.e. more flexibility). Additionally, the isolated C2A and C2B domain free energies of stability (which report on the overall breadth of each domain's conformational ensemble) in the presence and absence of various ligands indicates a high degree of malleability (Table 2.6). This is typified by the 1.8- and 0.6-fold changes in stability of C2A (in the presence of Ca^{2+} alone) and C2B (in the presence of PS alone), respectively. This malleability is enhanced when the two domains are tethered together and can be enhanced further still when a perturbation is introduced. For instance, the binding of Ca^{2+} ligand to the C2AB construct changes Δg_{int} from -1.8 kcal/mole to -3.9 kcal/mole. In other words, C2A and C2B are even less stable together than apart when in the presence of Ca^{2+}. Qualitative application of the fluctuation dissipation theorem provides an additional representation for this malleability, showing ligand-induced changes in the relative positions of native and denatured enthalpy distributions (supporting material, Fig. 2.2)[44]. Overall, this degree of flexibility is likely to make C2AB highly sensitive to other binding partners in its immediate environment, a trait conceptually consistent with a calcium sensor[35].

The differential binding preferences of each C2 domain can, however, modulate Δg_{int}. In the presence of PS alone (which had an overall destabilizing effect, decreasing C2AB's free energy from 2.24±0.01 kcal/mole to 1.74±0.01 kcal/mole), Δg_{int} did not change within error (went from -1.8 kcal/mole to -1.83 kcal/mole). Here, the binding of PS to C2A does not appear to have as great of a destabilizing effect on the adjacent C2B domain. If, however, Ca^{2+} ligand is added to drive the C2A domain into a lipid bound state, the degree of C2B destabilization becomes more pronounced as revealed by the FLT denaturations of C2AB under PS and Ca^{2+} conditions (Fig. 2.6K). Two of C2AB's three tryptophan residues are likely to be exposed to solvent (Fig. 2.9) and the third residue is partially buried in the hydrophobic environment between the two sheets of C2B's β-sandwich motif. As a result, the FLT denaturation method should report mostly on the stability of C2B in the C2AB construct[56]. The lack of a discernible transition under these conditions suggests that Ca^{2+} and PS destabilize C2B through negative coupling to such an extent that its β-sandwich tryptophan cannot articulate typical signal change during the unfolding process.

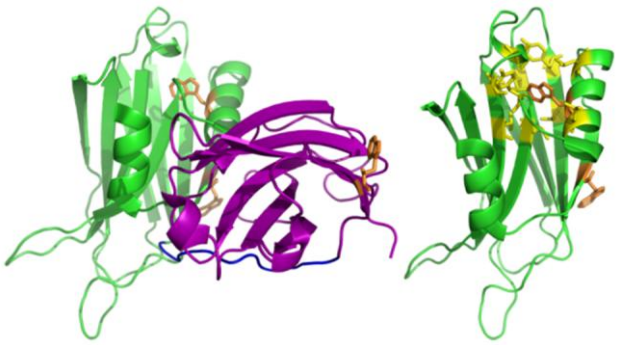

Figure 2.9 Location of tryptophan residues (orange) in C2A (purple) and C2B (green). Two of three tryptophan residues (C2A's and one of C2B's) occupy superficial positions and may, as a result, be more solvent exposed in solution (left). The second

tryptophan in the C2B domain is partially embedded in the core of the β-sandwich motif amongst several hydrophobic residues (yellow) (right). The differences in tryptophan environment likely give rise to unequal FLT signal contributions, with most of the signal coming from C2B's β-sandwich residue.

DSC denaturations of C2AB under the analogous PS and Ca^{2+} conditions lend further support to the negative coupling hypothesis. C2B, presumably the first peak in the heat capacity profile of Figure 2.6H (compare panels Fig. 2.4D and Fig. 2.6H), was far less prominent than C2A in the heat capacity profile. Furthermore, the fact that Fig. 2.6H shows two peaks is, in itself, an illustration of inter-domain coupling modulation. In other words, if strong coupling is present, one peak is seen; if weak coupling is present, two peaks are seen[34]. The C2AB construct unfolds as one coalesced peak under all conditions involving a single ligand, indicating that the energetic parameters describing C2AB combine in a way that facilitates coupling. The combination of PS and Ca^{2+} ligands will, however, modulate the energetic parameters of coupling so that two peaks start to become visible in the denaturation profile.

In contrast to the change in free energy brought about by binding of PS, PIP_2 had an overall stabilizing effect in the C2AB construct (as indicated by the increase in free energy from 2.24±0.01 to 2.56±0.01 kcal/mol). There were, however, discrepancies between DSC and FLT denaturation profiles. We attribute these differences to the sensitivity of FLT to microenvironment. Because PIP_2 is a specific ligand for C2B, its binding might select for a subset of conformers in which more water is excluded from the β-sandwich interior. This in turn might make the corresponding tryptophan residue

shown in Figure 2.9 (Trp 390) more sensitive to changes in solvation in response to increasing temperature and thus account for an early unfolding transition relative to DSC. In the case of PIP_2 and Ca^{2+} where the DSC profile is somewhat suggestive of independent domain unfolding, not seeing two independent transitions on FLT may be the result of unequal tryptophan signal contribution. Because PIP_2 is a ligand for C2B, it binding would presumably destabilize C2A through negative coupling, an effect perhaps accentuated by the additional presence of calcium ion[57]. The already superficial tryptophan on C2A (Trp 259) would be even less likely to report on the folded state of C2A.

In this denaturation study, two distinctly different techniques were used to monitor the unfolding transition of each protein construct. The intent of using both DSC (which provides a global perspective) and FLT (a more local perspective) was to overcome any inherent bias of using a single technique in isolation. When comparing the global fit of all DSC and FLT replicates to each individual method, minor deviations of the model were observed in DSC plots of the individual C2 domains. These observations suggest that, indeed, neither technique fully captures the unfolding transition on its own. In the case of C2AB, the unique perspective of each denaturation method is particularly prominent, as noted above. By including both DSC and FLT data sets in the global fit, these unfolding transitions are more completely described. Furthermore, the global fit approach is validated by the close agreement of calculated and calorimetric enthalpies ($\Delta H_{Tm}/\Delta H_{cal}$ ratio in Table 2.6). For both C2A and C2AB, this ratio was near unity. The higher $\Delta H_{Tm}/\Delta H_{cal}$ ratio of C2B indicates that its unfolding transition has a greater degree of complexity. However, the global two-state model still provides a quantitative estimate

of stability and will not change the overall finding of negative coupling and its implications on protein function.

When considering the work presented here, it is important to note how the approach used and the results obtained differ from those of previous experimentation looking at domain interaction of Syt I. Both the free energy of stability and free energy of interaction are global perspectives of Syt I behavior. As such, any specific structural contact points[28-29] that underlie the apparent malleability of negative coupling are included within Δg_{int}. The methodology employed here does not assign defined structural pathways of signal transduction, it encompasses them. In the previous domain interaction studies where no interaction was identified[20,30], the biophysical methods employed may not have been ideally suited for detecting the small energetic value of Δg_{int}. By approaching the question of domain interaction through stability determination as in this study, the small energetic value was more readily apparent because the free energies measured simply did not add up.

With these distinctions in mind, the above observations and thermodynamic profiles can introduce additional insight into Syt I function. The small energetic values of both $\Delta G°_{37°C}$ and Δg_{int} suggest sensitivity not only to endogenous such as Ca^{2+} and lipid, but also structural changes within the protein, like those that arise from gene mutation. Indeed, Syt I's functional sensitivity to mutation has been well documented[5-6,58]. However, point mutations may, as suggested in earlier *in vitro* work[31], negatively impact more than their original intended target. Specifically, point mutations may disrupt inter-domain coupling. This possibility makes assigning adverse physiological affects to what were originally perceived as being localized disruptions difficult because the nature of

inter-domain coupling is not local; the free energy terms that facilitate coupling, as they relate to conformational redistribution, are global. A point mutation that interferes with C2B's membrane binding ability, for instance, would not only disrupt that specific binding event, but also the way in which binding is coupled to modulation of the adjacent C2A domain. Though the C2A domain is not mutated, its function would still be impaired. Recent *in vitro* work, wherein a single C2B point mutation significantly disrupted the otherwise fast synchronous fusion of synthetic fluorescence vesicles in response to injected Ca^{2+}, is consistent with this notion[59]. α-synuclein, another allosteric neuronal protein that exhibits a similar form of coupling to C2AB, further exemplifies this type of global sensitivity[51]; oxidation of tyrosine residues far from α-synuclein's lipid binding domain disrupts the protein's ability to bind membrane. When elucidating functionality through mutation, these global effects should be considered.

Within the context of normal neurotransmission, the large and malleable conformer ensemble of Syt I has further functional implications. If the conformer ensembles of C2A and C2B are subject to modulation by ligands, they may, by extension, be influenced by other domain-specific binding partners in the immediate vicinity within the cell. Indeed, recent EPR and FRET studies looking at Syt I interactions with SNARE proteins show that even when bound to the SNARE complex, structural fluctuation and conformer heterogeneity still exist, indicating yet another possible means for modulating the Syt I conformer ensemble[60-61]. Experimental evidence on transcriptional protein systems that employ similar models for coupling support this possibility, showing that non-ligand binding partners can exert allosteric influence[53-54]. Accumulating experimental evidence for the convergence of lipid, Ca^{2+}, and fusion machinery proteins

on Syt I has long suggested a regulatory role[7,62-63]. By being marginally stable, Syt I may have such capacity, coordinating the molecular events of fusion using the inversely inter-linked, malleable properties of both domains to interact differentially with the wide array of binding partners encountered throughout fusion[64]. This hypothesis, constrained both by the thermodynamic evidence presented here and by extensive experimental data from the synaptotagmin field[5-6,11,18,24-28,31-32,58-61,65], may provide the necessary integrative means for Syt I-mediated neurotransmitter release.

Chapter 3: Allostery and instability in functional plasticity of synaptotagmin I

3.1 – Neural plasticity as a model for synaptotagmin I function*

The nervous system is known for its plasticity, both in development when synapses are being directed and connected and in life, as occurs with learning, memory, and emotion.[66-68] This plasticity of the nervous system is part of what enables great human diversity in response to stimuli. With this type of global behavior, it might be expected that the component parts of the nervous system function in analogous ways, which may be the case in the neuronal cell membrane.[69] The weak interaction energies between membrane lipids create a dynamic surface that allow for the possibility of protein-induce reorganization, a potential mechanism for mediating several cellular signaling events through domain formation.[70-72] Weak energetics, in this case, are what enable membrane plasticity and environmental responsiveness.[73] In addition to the membrane, there may also be plasticity in the proteins that mediate neuronal activity. Synaptotagmin I (Syt I), a key regulatory protein responsible for sensing the calcium ion (Ca^{2+}) influx that triggers neurotransmitter release,[5,11,18] may be one such example.

Like the immensely diverse neuronal networks that develop from a limited set of neuronal genes, the origins of Syt I's diverse *in vivo* functionality is not fully understood.[7,74] How Syt I is able to mediate vesicle docking, regulate SNARE complex function, enhance membrane disruption, facilitate vesicle and plasma membrane fusion, and participate in the reuptake of synaptic vesicles is at odds with our current view of neuronal protein function.[7,75-77] Recent experimental evidence may, however, shed light

* Note: This chapter was reproduced in its entirety under the terms of the Creative Commons Attribution License from the following open-access article: Fealey ME, Hinderliter A. Allostery and instability in the functional plasticity of synaptotagmin I. Commun Integr Biol 2013;6:e22830

on how Syt I accomplishes these numerous but related cellular tasks.[35,78] Much like the proposed selective stabilization of neuronal connections in developing networks[74,79] and the refinement of neural circuits with environmental input,[66,68,80] Syt I function may be the result of a molecular-level stabilization and refinement. In this neural plasticity analogy, Syt I's "primary connectivity" stems from the genetic code which provides a primary amino acid sequence that ultimately gives rise to a protein structure of low thermodynamic stability (and, consequently, a wide range of possible conformations).[81-82] Protein conformers imparted with important biological functions are selectively stabilized (or induced) by ligand and their function further refined by additional binding partners in the immediate cellular microenvironment.

3.2 – Allostery and instability: possible origins of Syt I plasticity

The basis for the above analogy stems from recent experimental observations of Syt I; namely, that the protein's two C2 domains (C2A and C2B) are marginally stable and negatively coupled.[35,78] By discussing how each domain's conformation changes as a result of both intrinsic properties during two theoretical binding events, a possible origin for Syt I's functional plasticity (that is physiologically consistent with the gross and microscopic features of the nervous system) can be seen. The discussion starts within a Monod-Wyman-Changeux (MWC) context of allostery.[83-85]

In their unbound form, both C2 domains have some basal level stability. When the first domain-specific ligand or binding partner binds to the C2B domain, for example, its free energy of stability is increased. Because the domains are negatively coupled, however, the opposite effect is seen in C2A; C2A's free energy decreases and gives the domain a higher degree of conformational flexibility. When the stability of the C2A

domain is lower, the energetic barrier between different conformations is lower. This allows the domain to more easily access conformers in the ensemble that were originally occupied with low probability (Fig. 3.1, top panel). If the now more readily accessible conformers are binding competent, their higher probability of being occupied will facilitate ligand binding (higher probability of binding-competent conformers is indicated in Figure 3.1 by the appearance of sites in the protein model depicted in the upper left corner of each panel. Note that the appearance of a binding site in this MWC context serves only to indicate the increased probability of a binding-competent conformer; though not initially shown in the model, those binding-competent conformers would always be present in the ensemble). As ligand binds, the binding-competent conformer is removed from the conformational equilibrium. To replenish this depleted conformer, the equilibrium of the ensemble shifts and more of the binding-competent conformer becomes available for additional ligation. The cycle of binding, conformer removal, and equilibrium shifting repeats ultimately resulting in the re-weighting of all conformers in the ensemble. Conformers that were of low initial probability may become more populated.

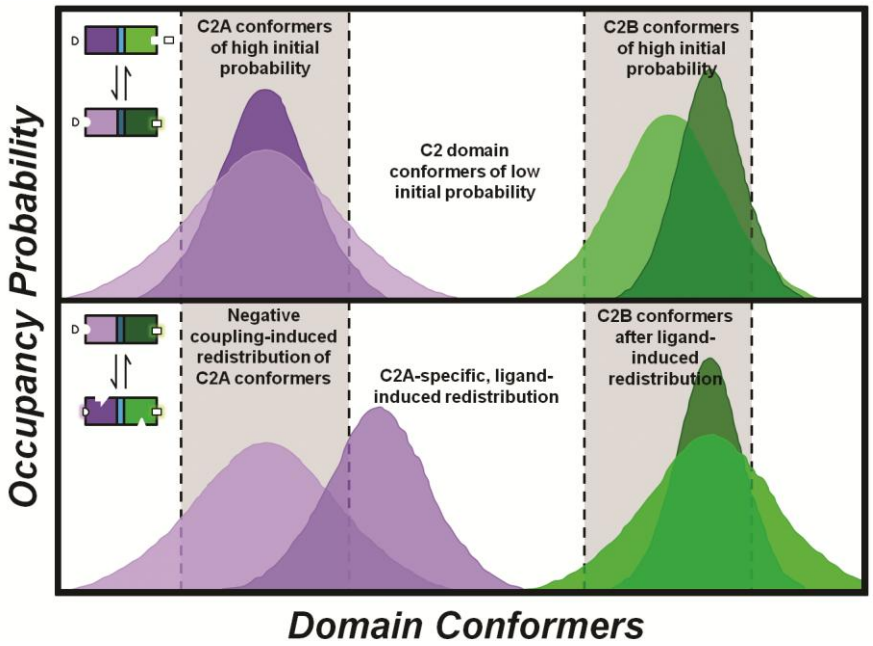

Figure 3.1 Conceptual representation of negative coupling- and ligand-induced redistribution of C2 domain conformers. *Top panel:* Initially, C2A (purple) and C2B (green) have basal level stability and corresponding distributions of conformers (note: colors correspond to models in upper left corner of diagram). Upon binding of a C2B-specific ligand or binding partner, both conformer distributions change (dark purple to light; light green to dark). The resultant change weights conformers in each domain's ensemble differently, allowing for C2A conformers that are initially less populated to become more significantly populated. *Bottom panel:* The more accessible conformers in the destabilized C2A domain, if binding-competent, can be selectively stabilized by ligand (or other binding partners) resulting in a ligand-induced redistribution of conformers (light purple to dark). This selective stabilization of C2A conformers simultaneously drives ensemble broadening in the adjacent C2B domain (dark green to light) through negative coupling. The end result of the negative coupling- and ligand-

induced redistribution inter-play is different combinations of domain conformer subsets for mediating different molecular events of neurotransmitter release.

Because Syt I's C2 domains have inter-linked ensembles, however, the ligand-induced redistribution in C2A not only stabilizes a subset of its own domain conformers, it also lowers the energetic barrier between the conformers of C2B through negative coupling (Fig. 3.1, bottom panel). Since the first binding event redistributed C2B's ensemble, the C2A-induced destabilization allows for a different subset of conformers (which may have different molecular ramifications) to become more accessible compared to C2B's basal state ensemble.

Alternatively, these two intrinsic properties can also be discussed within a Koshland-Némethy-Filmer (KNF) context of allostery.[86] Since C2A and C2B have marginal stability, the ease with which ligands or binding partners cause a structural change in Syt I increases. When the first ligand or binding partner binds to C2B, it causes a local conformational change in that domain. This change in local structure of C2B is subsequently communicated to C2A through the C2 domain interface. Because the interaction between the two domains is destabilizing, C2B causes C2A to become weaker allowing the C2A domain to take on new conformations not initially possible with basal stability (referring back to the bottom panel of Figure 3.1, this time in a KNF context, the appearance of binding sites in the Syt I model results from ligand- and/or binding partner-induced conformational changes of each domain). Because the C2A domain can now adopt these new conformations, it can bind to an additional ligand or binding partner. When this ligand or binding partner binds C2A, however, another local conformational

change occurs. This conformational change is not only communicated to the C2B domain through the destabilizing interaction that is negative coupling, but may also induce new binding sites within the C2A domain itself.

In either case of allostery, the end result of these two intrinsic protein properties is combinations of domain conformers that vary continuously with each ligand and binding partner. Just as weak energetics underlies the plasticity and responsiveness of the membrane, similar features seem to be present in Syt I.

3.3 – Dynamic shifting of conformer distributions and diversity of function

The illustrative example of shifting conformer distributions (MWC model) and changing conformations (KNF model) described above starts to show the conformational plasticity of Syt I with two theoretical binding events. When considering the number of ligands (Ca^{2+}, phosphatidylserine, phosphatidylinositol) and binding partners (SNAP-25, syntaxin, synaptobrevin, complexin) known to interact with each C2 domain and that do so differentially, the complexity of conformational change increases. When expanding the scope further still to incorporate influence from other lipid and protein species present in both vesicle and plasma membranes as well as the cytosol, the intricacy of conformational changes are staggering. If within each C2 domain's conformational repertoire there are distinct conformer subsets that mediate different molecular events of neurotransmission,[87] then ligand and binding partner-induced selections of domain conformer combinations (with subtle refinements from other constituents of the protein's microenvironment) may permit the nuanced functions of Syt I observed *in vivo*.[7,75-76] It is in this molecular stabilization and subtle refinement of conformers, enabled by allostery and instability, that Syt I mimics nervous system plasticity.

Chapter 4: Disorder conveys cooperativity: a functional fine-tuning role for the synaptotagmin linker

4.1 – Introduction

The synaptotagmins represent a large, differentially distributed family of proteins that regulate vesicle trafficking, most notably calcium (Ca^{2+})-triggered exocytosis [88]. Irrespective of cell type, vesicle size, membrane localization, and trafficking directionality of the vesicle, synaptotagmin proteins mediate this basic cellular process with the same overall structure: a short luminal segment (for those embedded in vesicle membranes), a transmembrane helix, a long cytosolic linker, and two tandem C2 domains (C2A and C2B). While this general structure is highly conserved amongst synaptotagmins and is thus crucial to normal protein function [89], the linker region that connects the C2 domains to the membrane exhibits substantial variability in length, sequence, and in some instances alternative splicing patterns (Figure 4.1). Such cellular attention to the variability of this portion of the protein is undoubtedly relevant to the behavior of each synaptotagmin isoform [90-93], but without some basic understanding of the linker's properties, potential mechanisms for functional diversification will remain poorly understood.

Syt I
KKCLFKKKNKKKGKEKGGKNAINMKDVKDLGKTMKDQALKDDDAETGLTDGEEKEEPKEEEKL
GKLQYSLDYDFQN

Syt II
CKKCCCKKKKNKKEKGKGMKNAMNMKDMKGGQDDDDAETGLTEGEGEGEEEKEPENL

Syt III
GGSAVGGGPLRKDLGPGVGLAGLVGGGGHHLAAGLGGHPLLGGPHHHAHAAHHPPFAELLEPGS
LGGSDTPEPSYLDMDSYPEAAAAAVAAGVKPSQTSPELPSEGGAGSGLLLLPPSGGGLPSAQSHQQ
VTSLAPTTRYPALPRPLTQQTLTSQPDPSSEERPPALPLPLPGGEEKAKLIGQIKPELYQGTGPGGRR
SGGGPGSGEAGTGA

Syt V
CCFCLYRKSCRRRTGKKSQAQAQVHLQEVKGLGQSYIDKVQPEVEELEPAPSGPGQQVADKHEL
GRLQYSLDYDFQSG

Syt VII
CHWCQRKLGKRYKNSLETVGTPDSGRGRSEKKAIKLPAGGKAVNTAPVPGQTPHDESDRRTEPRS
SVSDLVNSLTSEMLMLSPGSEEDEAHEGCSRENL

Syt IX
SWKLCWVPWRERGLPSGSKDNNQEPLNYMDTETNEQENSEDFLDPPTPCPDSSMKISHTSPDIPLS
TQTGIQENCAHGVRVQRQVTEPTSSARHNSIRRQLNLSNPDFNIQQLQKQEQLTGIGRIKPELYKQR
SLDNDDGRRSNSKAC

Syt X
WKLCWPCWKSKPVTSNITTLPQSISSAPTEVFETEEKKEIKENEKPAVKAIEPAIKISHTSPDIPAEVQ
TALKEHLIKHARVQRQITEPTSSTRHSSFRRHLPRQMQVSSVDFSMGTEPVLQRGETTTSIGRIKPEL
YKQKSVDSEGNQNEDVKIC

Figure 4.1 Extensive variability of synaptotagmin linkers. When looking at the sequences listed in this figure, there are clear differences in both length and number as well as distribution of charged (orange), polar (blue), and structure breaking (green) residues. All residues sequences start from the first amino acid emerging from the membrane and end just prior to the first C2 domain.

When looking at the linker region of several synaptotagmin isoforms, we noticed that while the length and residue sequence lack conservation, there is one apparent commonality: the overall percentage of charged, polar, and structure breaking amino acids is consistently high (Table 1). Additionally, the frequency of bulky hydrophobic residues (those that typically form the core of a globular domain) is low. Such a residue composition closely resembles that described for intrinsically disordered proteins [81-82,94]. Moreover, the apparent bias towards disorder-favoring residues regardless of linker length and species is hallmark of conserved linker disorder [81-82,95]. Disorder in an exocytotic context is fitting as most synaptotagmins are thought to interact with numerous protein and lipid mediators to facilitate vesicle and plasma membrane fusion

[17,22,24-27]. Disorder provides a potential integrative means for these interactions, conferring upon its host protein large capture radii for binding partners, high specificity and low affinity interactions, and a high degree of plasticity both structurally and (in the case of densely charged disorder regions) electrostatically [95-96]. Furthermore, disorder is well correlated with basic cell signaling and regulation pathways [97]. All of the above features make disorder an attractive, yet apt, tool for potential exploitation during the rapid, transient, and nuanced molecular events of exocytosis.

Isoform (species)	**Charged***	**Polar Uncharged***	**Structure Breaking***	**Total Disorder Promoting Residues**
Syt I (H. sapiens)†	38/76 (50%)	11/76 (14%)	11/76 (14%)	79%
Syt I (C. elegans)‡	33/78 (42%)	12/78 (15%)	14/78 (22%)	76%
Syt I (R. norvegicus)†	38/76 (50%)	11/76 (14%)	11/76 (14%)	79%
Syt I (M. musculus)†	38/76 (50%)	11/76 (14%)	11/76 (14%)	79%
Syt I (D. melanogaster)†	33/71 (46%)	12/71 (17%)	9/71 (13%)	76%
Syt I (G. gallus)‡	37/76 (49%)	11/76 (14%)	11/76 (14%)	78%
Syt I (B. taurus)†	35/63 (56%)	7/63 (11%)	10/63 (16%)	83%
Syt I (A. californica)†	28/62 (45%)	10/62 (16%)	8/62 (13%)	74%
Syt II (H. sapiens) †	29/57 (51%)	7/57 (12%)	11/57 (19%)	82%
Syt II (M. musculus) †	32/68 (47%)	10/68 (15%)	12/68 (18%)	79%
Syt II (R. norvegicus)†	32/68 (47%)	10/68 (15%)	12/68 (18%)	79%
Syt III (H. sapiens)‡	37/212 (17%)	37/212 (17%)	96/212 (45%)	80%
Syt III (R. norvegicus)†	42/224 (19%)	38/224 (17%)	94/224 (42%)	78%
Syt III (M. musculus)†	42/223 (19%)	38/223 (17%)	93/223 (42%)	78%
Syt V (H. sapiens) ‡	23/78 (29%)	17/78 (22%)	15/78 (19%)	71%
Syt V (R. norvegicus)†	25/78 (32%)	17/78 (22%)	11/78 (14%)	68%
Syt V (M. musculus)†	26/78 (33%)	18/78 (23%)	10/78 (13%)	69%
Syt VII (H. sapiens)	33/99 (33%)	23/99 (23%)	21/99 (21%)	78%
Syt VII (M. musculus)†	33/99 (33%)	24/78 (24%)	21/99 (21%)	79%

Syt IX (H. sapiens)‡	41/148 (28%)	50/148 (34%)	22/148 (15%)	76%
Syt IX (M. musculus)†	41/148 (28%)	49/148 (33%)	24/148 (16%)	77%
Syt IX (R. norvegicus)‡	41/148 (28%)	49/148 (33%)	24/148 (16%)	77%
Syt X (H. sapiens)‡	48/156 (31%)	45/156 (29%)	23/156 (15%)	73%
Syt X (R. norvegicus)‡	51/156 (33%)	41/156 (26%)	25/156 (16%)	75%
Syt X (M. musculus)†	51/156 (33%)	40/156 (26%)	25/156 (16%)	74%

Table 4.1 Distribution of disorder favoring residues in synaptotagmin. Note: * indicates the number of charged, polar uncharged, and structure breaking residues over the total number of residues in the linker region. The linker region for each isoform was assumed to include all residues between the transmembrane helix and first C2 domain. Residues that were considered structure breaking were glycine, proline, and alanine, as defined for intrinsically disordered proteins [81-82,94]. All sequences used were obtained from the Universal Protein Resource database. Note: † indicates amino acid sequence has evidence at protein level and ‡ indicates sequence evidence at transcript level.

To look for linker disorder in this context, we chose to study the best characterized isoform of the synaptotagmin family: synaptotagmin I (Syt I), the putative Ca^{2+} sensor for neuronal exocytosis [11,13,18,98]. Despite extensive study, the main properties that impart Syt I with the ability to change, transduce, and amplify the Ca^{2+} signal required for exocytosis have remained elusive. We have proposed that those main properties stem from marginal stability [35], a property that not only provides a means for easy dissemination of binding information, but also a means for cooperative ligand binding [12]. Both C2 domains of Syt I are marginally stable, but more importantly they are even less stable together due to negative coupling [78]. Such findings underscore the

importance of instability in this protein's Ca^{2+} sensing and signaling functions [99]. Because of this apparent inverse relationship of stability and signaling capacity, we believe that intrinsic disorder, an extremum of the protein structure continuum, underlies Syt I's responsiveness.

To directly test for disorder and its potential impact on Syt I's main cellular function, Ca^{2+} sensing, we studied two constructs of the first C2 domain (C2A): a short construct that includes residues 140-265 and a long construct that includes most of linker residues (96-265). Through the combined use of differential scanning calorimetry (DSC), fluorescence lifetime spectroscopy (FLT), circular dichroism (CD), and isothermal titration calorimetry (ITC) we found that the linker region is disordered and that the disordered linker broadens C2A's conformational ensemble to enable a cooperative Ca^{2+} binding response in the absence of membrane. These findings suggest the linker region may do more than simply tether C2 domains to the membrane. Collectively, these findings suggest that one broad function for disordered synaptotagmin linkers may be the tuning of adjacent C2 domain activity through a redistribution of the conformational ensemble [100].

4.2 – Materials and Methods

4.2.1 – Materials

Potassium chloride (KCl) was Puriss-grade and 3-(N-morpholino)propanesulfonic acid (MOPS) and calcium chloride dihydrate were Biochemika grade from Fluka Chemical Corp. All buffers used were decalcified using Chelex-100 ion-exchange resin (Bio-Rad Labs).

4.2.2 – Purification of Human Syt I C2A Domain

Protein purification was carried out as previously described[35]. Briefly, short and long constructs of C2A were purified as a glutathione S-transferase (GST) fusion proteins using affinity chromatography, followed by removal of the GST domain. Final purity was determined to be >95% both by SDS-PAGE densitometry and a 260/280 ratio of <0.70, the latter of which indicates <5% nucleic acid contamination. Final concentrations were determined using a Nanodrop with an A280 extinction coefficient of 12090$cm^{-1}M^{-1}$ and 12950 $cm^{-1}M^{-1}$ for short and long constructs, respectively. To further verify the distinct size of each protein construct, purified short and long C2A were subjected to ion-trap mass spectrometry. Molecular weights were as expected for each version of C2A (Figures 4.3 and 4.4).

4.2.3 – Differential Scanning Calorimetry

DSC experiments were performed on a NanoDSC (TA Instruments, New Castle, DE) using protein concentrations of approximately 0.2-0.3 mg/ml and a scan rate of 1 °C/min. These scans were conducted in 20 mM MOPS, 100 mM KCl, pH 7.5 which was

chelexed to remove any trace Ca^{2+}. Those scans performed in the absence of Ca^{2+} contained 500 μM EGTA. Scans in the presence of Ca^{2+} used concentrations such that the protein's Ca^{2+}-binding sites were >95% saturated. By comparing measured enthalpies from two scans of the same sample, a percentage for reversible folding was determined.

4.2.4 – Fluorescence Lifetime Spectroscopy

FLT experiments were performed on a Lifetime Spectrometer (Fluorescence Innovations, Inc., Bozeman, MT) using protein concentrations of 0.03 mg/ml. These scans were conducted in buffered solution as described above. The lifetime spectrometer is specifically tuned to excite tryptophan residues. The intrinsic tryptophan fluorescence was monitored as a function of increasing temperature and an emission spectrum consisting of just the integrated intensity of the lifetime decay (no time-resolved or lifetime measurements were made in this study) was collected from 310 nm to 360 nm, and data collected at 340 nm was used in the analysis. When applicable, a background of 500 μM EGTA was used to ensure Ca^{2+}-free conditions. In scans containing Ca^{2+}, concentrations corresponded to >95% saturation. By comparing the integrated fluorescence intensity of the sample before heating and after cooling, a percent reversibility was determined.

4.2.5 – Circular Dichroism

Circular dichroism was performed on short and long C2A in 20 mM MOPS, 100 mM KCl, pH 7.5 buffer in a 0.1 cm quartz cuvette using a J-810 JASCO spectropolarimeter. Far-UV spectra were collected over a wavelength range of 200-260

nm. Data points were collected in 1 nm increments and averaged over 3 acquisitions. Spectra collected were corrected for any buffer contributions by subtracting a buffer scan from the corresponding protein scan.

4.2.6 – Isothermal Titration Calorimetry

ITC was carried out according to the same rigorous procedures recently described [101]. Briefly, protein samples were thoroughly degassed for 20 minutes and Nanodropped prior to loading into the sample cell. Calcium chloride dissolved in the same buffer as the protein was then loaded into the titration syringe. The instrument was allowed to equilibrate for 3 hours prior to stirring. All data collected was corrected by subtracting the heat of dilution from injecting Ca^{2+} into buffer.

4.2.7 – Analysis of Denaturation Data

The denaturation analysis was carried out as previously described [35,78].

4.3 – Supporting Material

A.

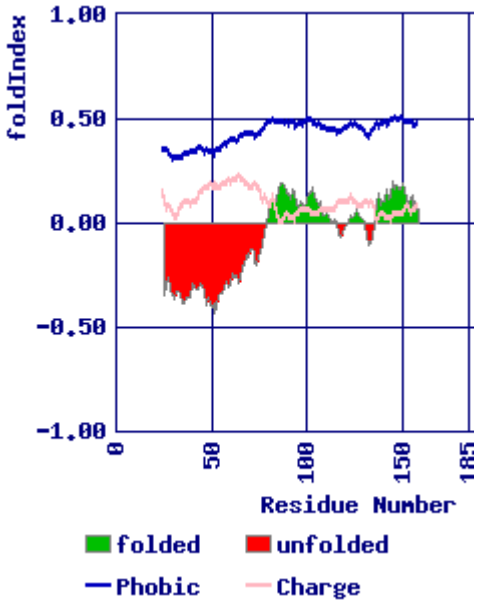


```
  1 KKCLFKKKNK KKGKEKGGKN AINMKDVKDL GKTMKDQALK DDDAETGLTD
 51 GEEKEEPKEE EKLGKLQYSL DYDFQNNQLL VGIIQAAELP ALDMGGTSDP
101 YVKVFLLPDK KKKFETKVHR KTLNPVFNEQ FTFKVPYSEL GGKTLVMAVY
151 DFDRFSKHDI IGEFKVPMNT VDFGHVTEEW RDLQS
```

(Predicted disordered segment)

B.

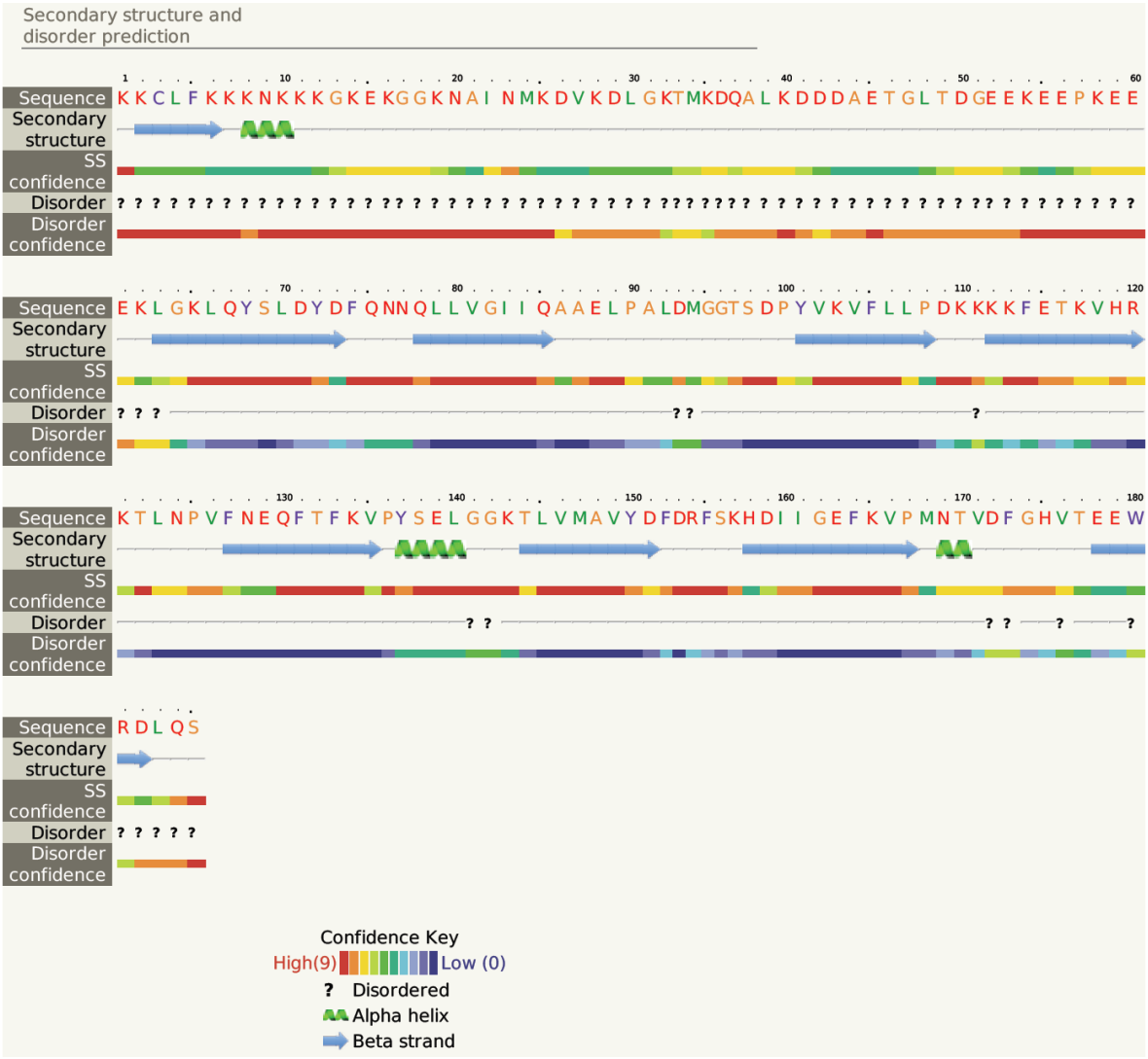
Secondary structure and disorder prediction
Sequence
Secondary structure
SS confidence
Disorder
Disorder confidence
Confidence Key
High(9) Low (0)
? Disordered
Alpha helix
Beta strand

C.

Predictor: VL3H

Window size: 11

Sequence:

KKCLFKKKNKKKGKEKGGKNAINMKDVKDLGKTMKDQALKDDDAETGLTDGEEKEE
PKEEEKLGKLQYSLDYDFQNNQLLVGIIQAAELPALDMGGTSDPYVKVFLLPDKKKKFE
TKVHRKTLNPVFNEQFTFKVPYSELGGKTLVMAVYDFDRFSKHDIIGEFKVPMNTVDFG
HVTEEWRDLQS

#	AA	VL3H											
1	K	0.928715	D	51	G	0.866088	D	102	V	0.218234	o	153	D 0.129315 o
2	K	0.925564	D	52	E	0.862151	D	103	K	0.231085	o	154	R 0.129424 o
3	C	0.923869	D	53	E	0.857672	D	104	V	0.244356	o	155	F 0.126749 o
4	L	0.921825	D	54	K	0.854490	D	105	F	0.262211	o	156	S 0.126109 o
5	F	0.919148	D	55	E	0.850728	D	106	L	0.273751	o	157	K 0.126547 o
6	K	0.917144	D	56	E	0.845173	D	107	L	0.285791	o	158	H 0.127564 o
7	K	0.914167	D	57	P	0.837073	D	108	P	0.297908	o	159	D 0.127009 o
8	K	0.910632	D	58	K	0.821044	D	109	D	0.318184	o	160	I 0.127343 o
9	N	0.907229	D	59	E	0.793451	D	110	K	0.336582	o	161	I 0.130096 o
10	K	0.904460	D	60	E	0.780093	D	111	K	0.349618	o	162	G 0.134115 o
11	K	0.900746	D	61	E	0.750692	D	112	K	0.360514	o	163	E 0.136550 o
12	K	0.897113	D	62	K	0.719629	D	113	K	0.377605	o	164	F 0.138747 o
13	G	0.893501	D	63	L	0.695510	D	114	F	0.389186	o	165	K 0.140664 o
14	K	0.888041	D	64	G	0.671392	D	115	E	0.403044	o	166	V 0.149818 o
15	E	0.884122	D	65	K	0.655909	D	116	T	0.409553	o	167	P 0.156575 o
16	K	0.880252	D	66	L	0.634183	D	117	K	0.425841	o	168	M 0.161965 o
17	G	0.873937	D	67	Q	0.613073	D	118	V	0.445830	o	169	N 0.166067 o
18	G	0.864675	D	68	Y	0.588234	D	119	H	0.457400	o	170	T 0.171255 o
19	K	0.857353	D	69	S	0.565790	D	120	R	0.462160	o	171	V 0.176004 o
20	N	0.852484	D	70	L	0.552434	D	121	K	0.466682	o	172	D 0.179154 o
21	A	0.849711	D	71	D	0.520438	D	122	T	0.467234	o	173	F 0.180456 o
22	I	0.847011	D	72	Y	0.494578	o	123	L	0.468311	o	174	G 0.185852 o
23	N	0.842031	D	73	D	0.471111	o	124	N	0.461366	o	175	H 0.187427 o
24	M	0.836619	D	74	F	0.442522	o	125	P	0.457423	o	176	V 0.188410 o
25	K	0.832198	D	75	Q	0.411055	o	126	V	0.439440	o	177	T 0.191720 o
26	D	0.825866	D	76	N	0.363579	o	127	F	0.422294	o	178	E 0.198585 o
27	V	0.820314	D	77	N	0.319358	o	128	N	0.396449	o	179	E 0.199916 o
28	K	0.817561	D	78	Q	0.277880	o	129	E	0.361113	o	180	W 0.205319 o
29	D	0.817827	D	79	L	0.240348	o	130	Q	0.333024	o	181	R 0.207242 o
30	L	0.818327	D	80	L	0.210555	o	131	F	0.302734	o	182	D 0.210308 o
31	G	0.816369	D	81	V	0.183229	o	132	T	0.276562	o	183	L 0.215487 o
32	K	0.811524	D	82	G	0.163050	o	133	F	0.246576	o	184	Q 0.223062 o
33	T	0.807217	D	83	I	0.151140	o	134	K	0.219615	o	185	S 0.228864 o
34	M	0.807444	D	84	I	0.141282	o	135	V	0.195962	o		
35	K	0.811175	D	85	Q	0.128593	o	136	P	0.170327	o		
36	D	0.816780	D	86	A	0.119158	o	137	Y	0.154999	o		
37	Q	0.824903	D	87	A	0.116756	o	138	S	0.145863	o		
38	A	0.834030	D	88	E	0.122261	o	139	E	0.142480	o		
39	L	0.843161	D	89	L	0.127277	o	140	L	0.141888	o		
40	K	0.851580	D	90	P	0.134330	o	141	G	0.140387	o		
41	D	0.857679	D	91	A	0.139617	o	142	G	0.141045	o		
42	D	0.864321	D	92	L	0.145905	o	143	K	0.138961	o		
43	D	0.870470	D	93	D	0.151774	o	144	T	0.140616	o		
44	A	0.877177	D	94	M	0.155434	o	145	L	0.140169	o		
45	E	0.880770	D	95	G	0.157474	o	146	V	0.140134	o		
46	T	0.884241	D	96	G	0.164722	o	147	M	0.140505	o		
47	G	0.883594	D	97	T	0.172687	o	148	A	0.142989	o		
48	L	0.881799	D	98	S	0.179995	o	149	V	0.142923	o		
49	T	0.876373	D	99	D	0.183252	o	150	Y	0.139960	o		
50	D	0.871498	D	100	P	0.196403	o	151	D	0.135218	o		
				101	Y	0.207326	o	152	F	0.131218	o		

D.

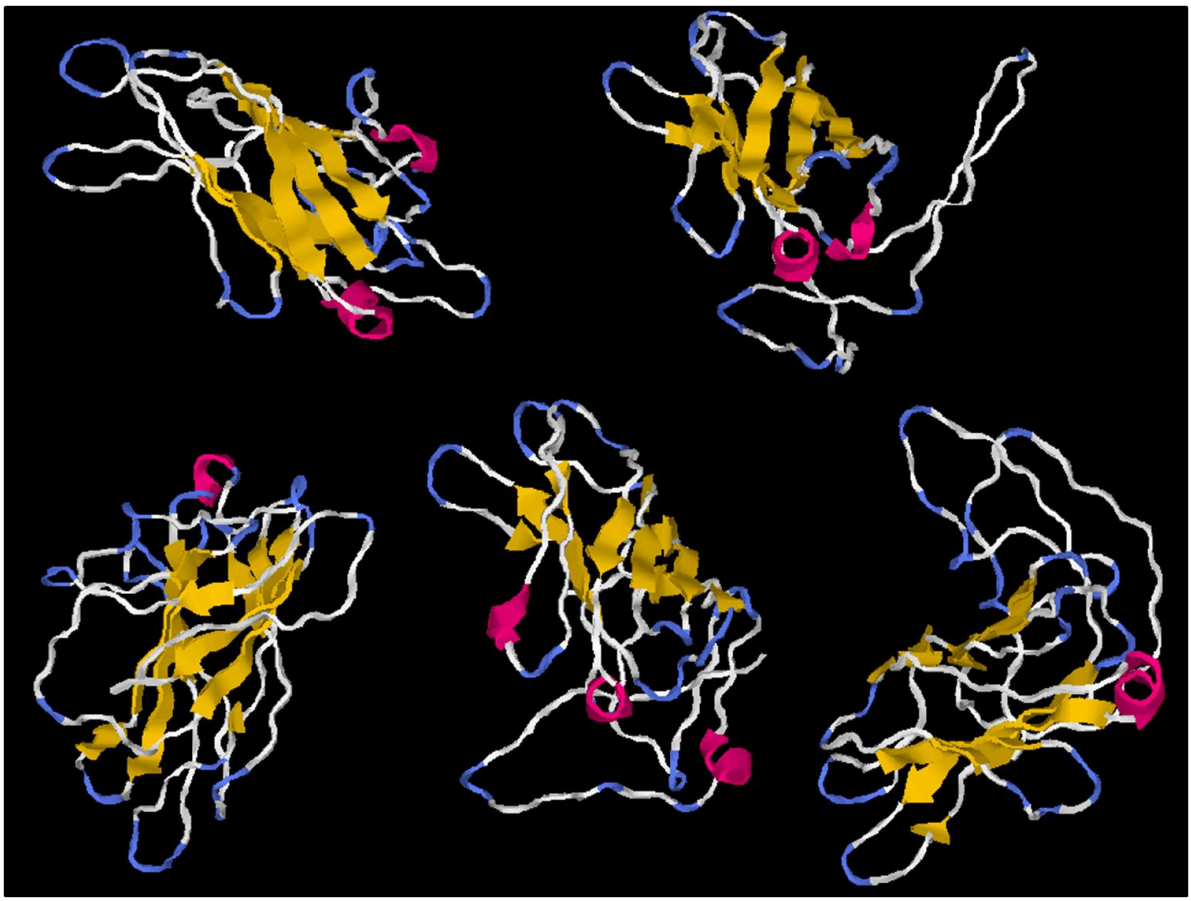

Figure 4.2 Predicted structure for linker region using different predictive programs. Several different protein structure and disorder programs including those of (A) FoldIndex [102], (B) Phyre[2] [103], (C) DisProt [104-105], and (D) I-TASSER [106] all converge on a similar finding: the linker region is likely disordered. This is suggested by either the program's direct disorder prediction or, as with I-TASSER, a multitude of different structure predictions for the linker region, consistent with a disordered region that can adopt several possible conformations.

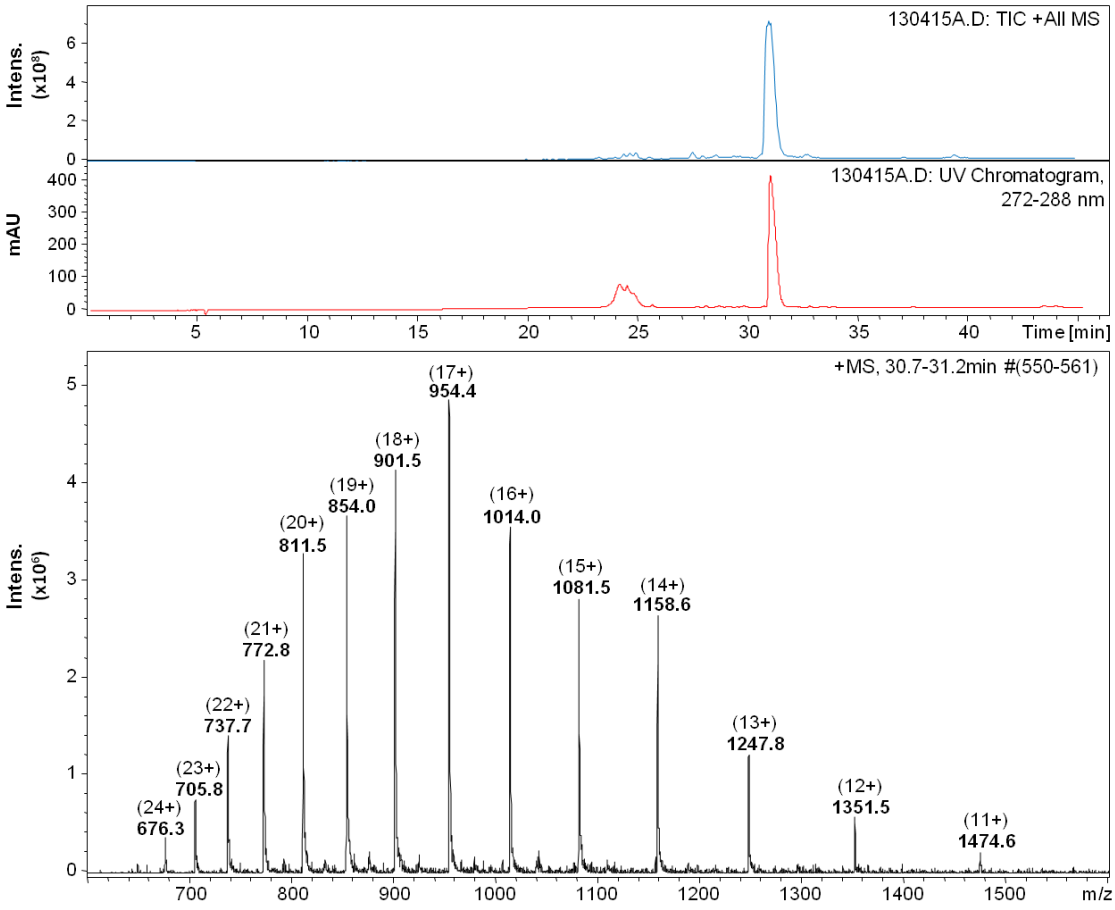

Figure 4.3 Representative mass spectrum for short C2A construct.

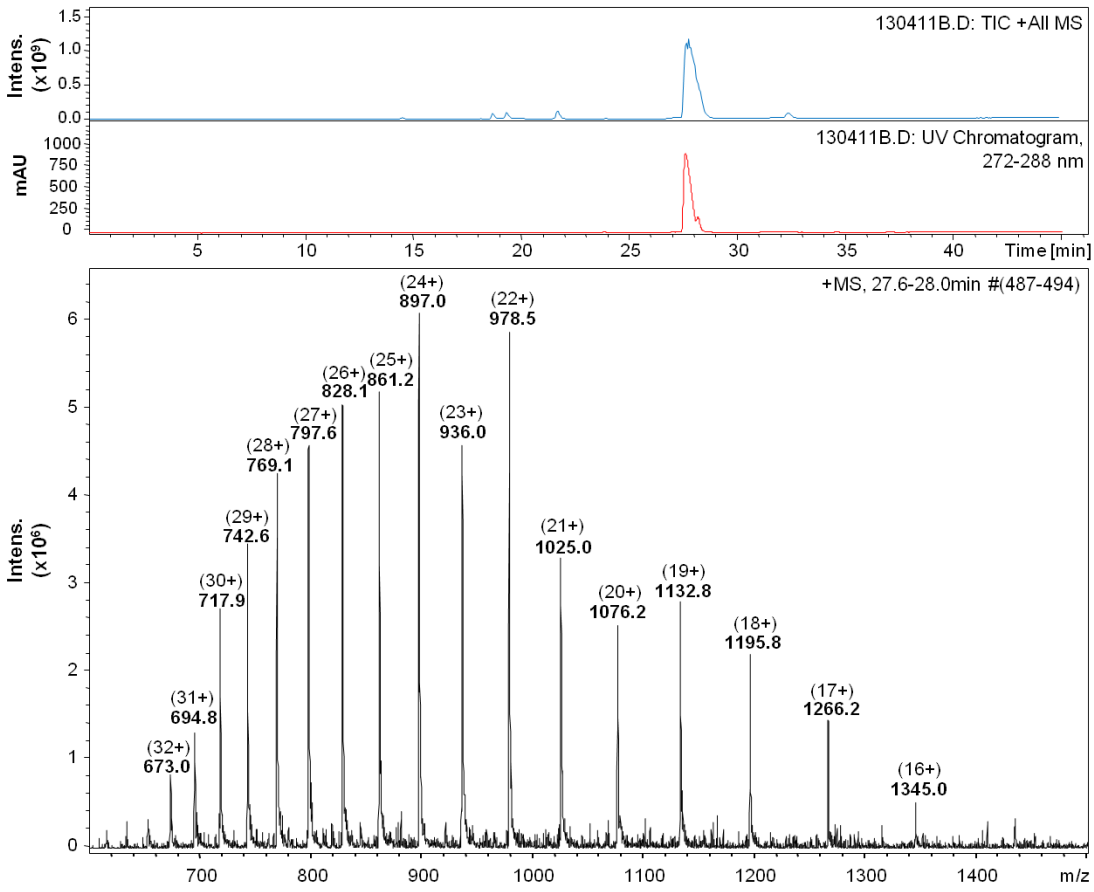

Figure 4.4 Representative mass spectrum for long C2A construct.

4.4 – Results

4.4.1 – Short and long C2A are both structurally and energetically distinct

To assess whether or not the linker had defined structure and if the linker changed the overall topology of C2A, the long C2A construct was crystallized and compared to the short structure previously solved (1BYN)[22]. Structurally, the short and long constructs of the C2A domain are very similar, with only two main differences (unpublished data). The first difference is simply that the linker residues of the long C2A construct were not visible in the crystal lattice, consistent with the region being disordered [107]. Indeed, when the long C2A sequence is subjected to several different structure-predicting programs, all predict either a lack of defined structure or disorder for the linker region (Figure 4.2 [102-105]). Both findings align with the linker region's high susceptibility to proteolytic cleavage, another common feature of disordered regions [108]. The second difference lies in the loops that form the Ca^{2+} binding sites.

While the crystallographic results suggest considerable similarity between constructs, a highly dynamic unstructured region should have some thermodynamic impact on the stability of the C2A domain. To directly test this hypothesis, the long construct of C2A was thermally denatured in the presence and absence of Ca^{2+} ligand (Figure 4.5). In comparison to the short C2A construct previously studied [35], long C2A was considerably weaker with a calorimetric enthalpy of 32.5±5.6 kcal/mole, an unfolding transition temperature of 55.5 °C, and a corresponding free energy of stability of 1.19 kcal/mole (the short C2A construct had an enthalpy of 58.7 kcal/mole, a transition temperature of 56.0 °C, and a corresponding free energy of stability of 2.23 kcal/mole). Moreover, where short C2A had a range of reversible folding between first and second

denaturation scans (60-90%), long C2A exhibited nearly complete reversibility (93%). The free energies measured for long C2A were, as seen previously [35,78], low for similar molecular weight proteins. Unlike the other Syt I constructs, however, the long C2A's overall change in heat capacity (ΔC_p) was markedly lower than expected (ΔC_p was anticipated to be between 1.92 and 2.54 kcal/mole [42] and the experimental value was 1.20 kcal/mole) suggesting the native state of long C2A has a greater degree of hydrophobic residue exposure compared to short C2A [109].

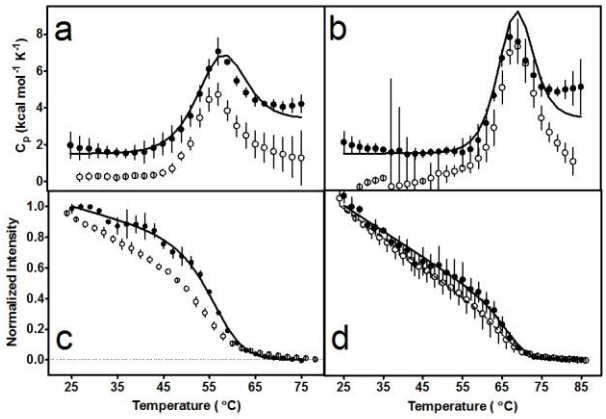

Figure 4.5 Thermal denaturation of short (●) and long (○) C2A using DSC (top panels) and FLT (bottom panels) methods. Short C2A denaturations are displayed with permission from Biophysical Journal[35]. Higher concentrations refer to DSC samples. (A, E) [short C2A] = 13 μM and 0.75 μM, [long C2A] = 12.5 μM and 0.75 μM in the presence of 500 μM EGTA. (B, F) [short C2A] = 13 μM and 0.75 μM, [long C2A] = 13.3 μM and 0.75 μM in the presence of Ca^{2+}. [Ca^{2+}] = 800 μM and 770 μM for short C2A, [Ca^{2+}] = 1 mM and 800 μM for long C2A. Short C2A denaturation data in isolation was originally used in a former graduate student's thesis, but was include here out of necessity as it is part of answering the research question at hand[48].

4.4.2 – Differences continue with divergent secondary structure

The difference in free energy of long and short C2A suggests that, despite crystallographic similarities, there should be some structural differences between constructs. To test this hypothesis, we performed circular dichroism to assess types of secondary structure present. In both the presence and absence of Ca^{2+} ligand, the secondary structure of short and long C2A differ considerably (Figure 4.6). The short construct exhibits a strong β-sheet signal as expected [110]. In contrast, long C2A has a stronger random coil contribution, consistent with the hypothesis of a disordered linker region. Interestingly, in the presence of saturating Ca^{2+}, the change in secondary structure is more pronounced with long C2A than short. Based on the lower thermodynamic stability of long C2A, we would expect the protein to be more responsive to ligand which, when looking at the way Ca^{2+} binding is propagated throughout the secondary structure in Figure 4.6d, seems to be the case. Such a change in long C2A secondary structure is consistent with the idea of weak energetics being more conducive to signal propagation. Short C2A's secondary structure looks nearly identical in the presence of saturating Ca^{2+}, consistent with previous crystallographic and solution NMR studies of this same construct [22,111].

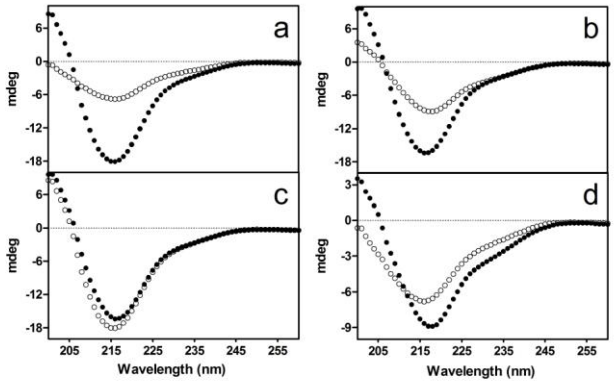

Figure 4.6 Circular dichroism comparison of short (closed circles) and long (open circles) C2A constructs. a) 30 μM long C2A and short C2A in the presence of 500 μM EGTA. b) 30 μM long C2A and short C2A in the presence of 1 mM Ca^{2+}. c) Overlay of short C2A in the presence (closed circles) and absence (open circles) of Ca^{2+}. d) Overlay of long C2A in the presence (closed circles) and absence (open circles) of Ca^{2+}.

4.4.3 – Linker-induced changes correlate with a difference in Ca^{2+} binding behavior

Knowing the linker changes both the stability and structure of the C2A domain, we anticipated a difference in binding behavior between short and long constructs. To test for this functional difference, the Ca^{2+} binding of short and long C2A constructs were investigated using ITC. Upon first inspection, the binding profiles of short and long C2A are noticeably different (Figure 4.7, left most panels). These binding profiles suggest the Ca^{2+} binding sites of the short construct are independent whereas the binding sites of the long construct are not. The long C2A binding profile is strongly suggestive of cooperative binding. Similar differences in binding profiles were seen previously in FRET binding studies using the Ca^{2+} mimic terbium [35,40].

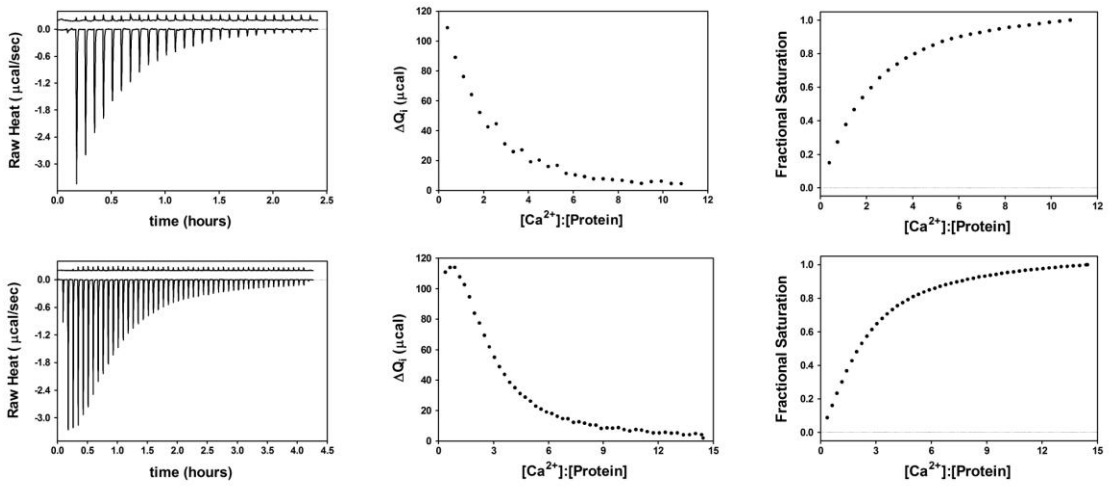

Figure 4.7 Isothermal titration calorimetry of short (top panels) and long (bottom panels) C2A constructs. The above panels show the raw heat of binding and associated heat of dilution (left), change in heat as saturation is approached (middle), and fractional saturation as a function of ligand (right) for both C2A constructs. The short C2A construct was at a concentration of 408 µM and was titrated with 15 mM Ca^{2+} at 15 °C. Injection volume was 1 µL for the first injection point and then 9 µL for all subsequent injections. The long C2A construct was at a concentration of 303 µM and was titrated with 14.5 mM Ca^{2+} at 15 °C. The injection volume for long C2A was 2 µL for the first injection then 5.14 µL for all remaining injections.

4.5 – Discussion

The purpose of the current study was to test for and assess the impact of intrinsic disorder on the Ca^{2+} sensing function of synaptotagmin. This was done using the first C2 domain of the best characterized family isoform, Syt I. Using a combination of calorimetry and spectroscopy we found that the linker region that normally tethers Syt I's C2 domains to the membrane is likely disordered and that this disorder confers upon the

C2A domain cooperative Ca^{2+} binding in the absence of membrane. These findings not only provide new insights into how Syt I sensitively detects Ca^{2+}, but also suggests that the linker region that is found in all synaptotagmins, but with substantial variability, may in part function to tune C2 domain activity.

In the Syt I construct studied here, the origin of long C2A's cooperative Ca^{2+} binding seems to stem from a lower thermodynamic stability as determined by DSC and FLT denaturation methods (Figure 4.5). The linker does not substantially change the native structure of C2A. Rather, the linker changes the way in which conformers of the C2A domain are populated (unpublished crystallography data and CD spectra of short and long C2A in Figure 4.6) [112]. When the linker is included in C2A, the Ca^{2+} binding competent conformers have a lower probability of being occupied because of the domain's decreased free energy of stability. This reduced occupancy in conjunction with cooperative binding of Ca^{2+} found through ITC (Figure 4.7) is consistent with the idea of transitioning from an unbound state to a state that has higher affinity for Ca^{2+}. This apparent linkage of instability and cooperative binding strongly suggests an allosteric transition model similar to that proposed by MWC [83] for Ca^{2+} binding with cooperativity between Ca^{2+} binding sites (not between subunits). For example, the singly-ligated state (C2A bound to one Ca^{2+}) could have higher affinity for binding of additional Ca^{2+}. Using of molecular partition functions and binding constants determined from previous Tb^{3+} binding studies of each C2A construct[35,40], this shift can be seen by plotting the fraction of singly- and doubly-ligated states as a function of ligand (Figure 4.8). As in the MWC model, the conformer that has higher affinity for ligand is sparsely populated and cooperativity comes from transitioning to the sparsely populated conformer. The short

C2A construct does not have a sparsely populated singly-ligated state. The conformational equilibrium does not favor the unbound state as significantly (compare long C2A K_1 = 3100 M^{-1} and short C2A K_1 = 50000 M^{-1}) and thus cooperativity between the first two Ca^{2+} sites is absent.

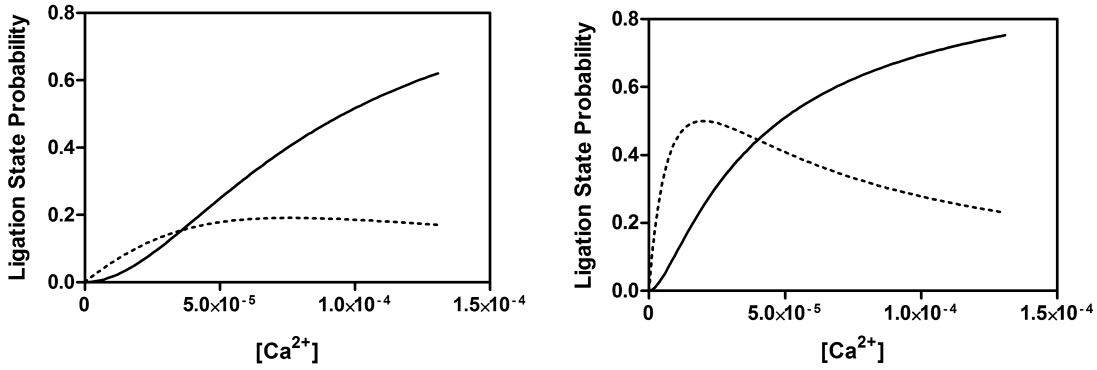

Figure 4.8 Dynamic shifting of conformer populations to facilitate cooperative response to Ca^{2+}. Using the partition functions and binding constants derived from terbium binding studies[35,40], plots were created to show how the probability of the singly- (dotted lines) and doubly-ligated (solid lines) states of C2A differ between long (left) and short (right) constructs. Because of long C2A's higher affinity for binding of a second Ca^{2+}, there is a cooperative binding curve for the doubly-ligated state as the conformational equilibrium shifts.

The disorder-induced changes in both binding and stability, when considered in a broader Syt I context, have interesting implications for how signals are propagated by this protein. Since the linker region influences the binding behavior of C2A and C2A influences C2B through negative coupling [78], signaling events mediated by Syt I are

propagated throughout the entire cytosolic region of the protein. Such a possibility is broadly relevant to the study of Syt I because it suggests that few protein and lipid interactions that occur throughout the cytosolic portion of the protein are likely to be completely independent of one another. Also of note is the disorder-induced reversibility of long C2A folding. The complete reversibility found for long C2A speaks to the plasticity of its structure. The implications are that C2A can adopt any possible conformation but still return to its native basal state ensemble. The same cannot be said for short C2A where the disordered linker is absent and reversible folding is greatly diminished. In the broader context of our Syt I model where ligands and binding partners select for conformer subsets that mediate different molecular events of exocytosis [35], such plasticity may underlie the protein's functional diversity [99]. By changing the way in which conformers are populated, as the disordered linker did for C2A in this study, a different functionality emerges. A similar observation was made for C2B and its membrane penetrating ability [113]. In the absence of the C2A domain, membrane penetration of C2B was absent; in C2A's presence, which changes the way in which C2B conformers are occupied because of negative coupling, the membrane penetrating ability of C2B appears. In both examples of emerging functionality there is an accompanying decrease in free energy that alters domain ensembles.

Considering the apparent conservation in linker disorder (Table 4.1) and the apparent change in functionality induced by the linker's presence (Figure 4.7), the data presented here suggests that one broad function of the synaptotagmin membrane-C2 domain linker may be to tune C2 domain functionality. If the linker broadens the ensemble (by lowering the thermodynamic stability) of each C2 domain and there are

new functionalities that emerge as a result, then the difference in length and residue composition may enable differentiated function.

Conclusion

The initial hypothesis that Syt I draws its signaling power from marginal stability and disorder is supported by the chapters presented in this thesis. The integrative capacity of Syt I can be seen with negative coupling. The cooperative interactions that exist between Syt I's C2 domains result from a destabilizing interaction free energy. The ability of C2A and C2B to integrate their binding information is thus facilitated by reduced stability. The impact of disorder on signaling can be seen with the comparison of short and long C2A constructs. Disorder greatly weakens the C2A domain and, in doing, tunes the calcium sensing functionality from a mode that lacks cooperativity to one that has cooperativity. Both findings are consistent the hypothesis that Syt I's signaling capacity and functional diversity are inversely related to protein stability. Based on the information presented here, it is hoped that this working model will provide a foundation for future study of Syt I's structural dynamics and how redistributions in the protein's conformational ensemble mediate all molecular roles in the events of neurotransmission.

REFERENCES

1 Fox, S. I. (McGraw-Hill, 2012).

2 Brunger, A. T. Structure of proteins involved in synaptic vesicle fusion in neurons. *Annu Rev Biophys Biomol Struct* **30**, 157-171 (2001).

3 Takamori, S. *et al.* Molecular anatomy of a trafficking organelle. *Cell* **127**, 831-846 (2006).

4 Geppert, M. *et al.* Synaptotagmin I: a major Ca2+ sensor for transmitter release at a central synapse. *Cell* **79**, 717-727 (1994).

5 Littleton, J. T., Stern, M., Perin, M. & Bellen, H. J. Calcium dependence of neurotransmitter release and rate of spontaneous vesicle fusions are altered in Drosophila synaptotagmin mutants. *Proc. Natl. Acad. Sci. USA* **91**, 10888-10892 (1994).

6 Littleton, J. T., Stern, M., Schulze, K., Perin, M. & Bellen, H. J. Mutational analysis of Drosophila synaptotagmin demonstrates its essential role in Ca2+-activated neurotransmitter release. *Cell* **74**, 1125-1134 (1993).

7 Chapman, E. R. How does synaptotagmin trigger neurotransmitter release? *Annu. Rev. Biochem.* **77**, 615-641 (2008).

8 Berridge, M. J., Bootman, M. D. & Roderick, H. L. Calcium signalling: dynamics, homeostasis and remodelling. *Nat Rev Mol Cell Biol* **4**, 517-529 (2003).

9 Berridge, M. J., Lipp, P. & Bootman, M. D. The versatility and universality of calcium signalling. *Nat Rev Mol Cell Biol* **1**, 11-21 (2000).

10 Clapham, D. E. Calcium signaling. *Cell* **131**, 1047-1058 (2007).

11 Fernández-Chacón, R. *et al.* Synaptotagmin I functions as a calcium regulator of release probability. *Nature* **410**, 41-49 (2001).

12 Hilser, V. J. & Thompson, E. B. Intrinsic disorder as a mechanism to optomize allosteric coupling in proteins. *Proc. Natl. Acad. Sci. USA* **104**, 8311-8314 (2007).

13 Chapman, E. R. Synaptotagmin: A Ca2+ sensor that triggers exocytosis? *Nat. Rev. Mol. Cell. Biol.* **3**, 1-11 (2002).

14 McMahon, H. T., Missler, M., Li, C. & Südhof, T. C. Complexins: cytosolic proteins that regulate SNAP receptor function. *Cell* **83**, 111-119 (1995).

15 Murthy, V. N. & De Camili, P. Cell biology of the presynaptic terminal. *Annu. Rev. Neurosci.* **26**, 701-728 (2003).

16 Südhof, T. C. The synaptic vesicle cycle. *Annu. Rev. Neurosci.* **27**, 509-547 (2004).

17 Tang, J. *et al.* A complexin/synaptotagmin 1 switch controls fast synaptic vesicle exocytosis. *Cell* **126**, 1175-1187 (2006).

18 Brose, N., Petrenko, A. G., Südhof, T. C. & Jahn, R. Synaptotagmin: a calcium sensor on the synaptic vesicle surface. *Science* **256**, 1021-1025 (1992).

19 Rogasevskaia, T. P., Churchward, M. A. & Coorssen, J. R. Anionic lipids in Ca(2+)-triggered fusion. *Cell Calcium* **In press** (2012).

20 Araç, D. *et al.* Close membrane-membrane proximity induced by Ca2+-dependent multivalent binding of synaptotagmin-1 to phospholipids. *Nat. Struct. Mol. Biol.* **13**, 209-217 (2006).

21 Fernandez, I. *et al.* Three-dimensional structure of the synaptotagmin 1 C2B-domain: synaptotagmin 1 as a phospholipid binding machine. *Neuron* **32**, 1057-1069 (2001).
22 Sutton, R. B., Davletov, B. A., Berghuis, A. M., Südhof, T. C. & Sprang, S. R. Structure of the first C2 domain of synaptotagmin I: a novel Ca2+/phospholipid-binding fold. *Cell* **80**, 929-938 (1995).
23 Zhang, X., Rizo, J. & Südhof, T. C. Mechanism of phospholipid binding by the C2A-domain of synaptotagmin I. *Biochemistry* **37**, 12385-12403 (1998).
24 Chapman, E. R., Hanson, P. I., An, S. & Jahn, R. Ca2+ regulates the interaction between synaptotagmin and syntaxin 1. *J. Biol. Chem.* **270**, 23667-23671 (1995).
25 Earles, C. A., Bai, J., Wang, P. & Chapman, E. R. The tandem C2 domains of synaptotagmin contain redundant Ca2+ binding sites that cooperate to engage t-SNAREs and trigger exocytosis. *J. Cell Biol.* **154**, 1117-1123 (2001).
26 Schiavo, G., Stenbeck, G., Rothman, J. E. & Söllner, T. H. Binding of the synaptic vesicle v-SNARE, synaptotagmin, to the plasma membrane t-SNARE, SNAP-25, can explain docked vesicles at neurotoxin-treated synapses. *Proc. Natl. Acad. Sci. USA* **94**, 997-1001 (1997).
27 Zhang, X., Kim-Miller, M. J., Fukuda, M., Kowalchyk, J. A. & Martin, T. F. J. Ca2+-dependent synaptotagmin binding to SNAP-25 is essential for Ca2+-triggered exocytosis. *Neuron* **34**, 599-611 (2002).
28 Fuson, K. L., Montes, M., Robert, J. J. & Sutton, R. B. Structure of human synaptotagmin 1 C2AB in the absence of Ca2+ reveals a novel domain association. *Biochemistry* **46**, 13041-13048 (2007).
29 Garcia, R. A., Forde, C. E. & Godwin, H. A. Calcium triggers an intramolecular association of the C2 domains in synaptotagmin. *Proc. Natl. Acad. Sci. USA* **97**, 5883-5888 (2000).
30 Huang, H. & Cafiso, D. S. Conformation and membrane position of the region linking the two C2 domains in synaptotagmin 1 by site-directed spin labeling. *Biochemistry* **47**, 12380-12388 (2008).
31 Wang, P., Wang, C.-T., Bai, J., Jackson, M. B. & Chapman, E. R. Mutations in the effector binding loops in the C2A and C2B domains of synaptotagmin I disrupt exocytosis in a nonadditive manner. *J. Biol. Chem.* **278**, 47030-47037 (2003).
32 Herrick, D. Z., Sterbling, S., Rasch, K. A., Hinderliter, A. & Cafiso, D. S. Position of synaptotagmin I at the membrane interface: cooperative interactions of tandem C2 domains. *Biochemistry* **45**, 9668-9674 (2006).
33 Lemmon, M. A. Membrane recognition by phospholipid-binding domains. *Nat. Rev. Mol. Cell Biol.* **9**, 99-111 (2008).
34 Luque, I., Leavitt, S. A. & Freire, E. The linkage between protein folding and functional cooperativity: two sides of the same coin? . *Annu. Rev. Biophys. Biomol. Struct.* **31**, 235-256 (2002).
35 Gauer, J. W. *et al.* Mechanism for calcium Ion sensing by the C2A domain of synaptotagmin I. *Biophys. J.* **103**, 238-246 (2012).
36 Freire, E. Differential scanning calorimetry. *Methods Mol. Biol.* **40**, 191-218 (1995).

37 Freire, E. The thermodynamic linkage between protein structure, stability, and function. *Methods Mol. Biol.* **168**, 37-68 (2001).
38 Montes, M., Fuson, K. L., Sutton, R. B. & Robert, J. J. Purification, crystallization and x-ray diffraction analysis of human synaptotagmin 1 C2A-C2B. *Acta. Crystallogr. Sect. F Struct. Biol. Cryst. Commun.* **62**, 926-929 (2006).
39 Kingsley, P. B. & Feigenson, G. W. The synthesis of a perdeuterated phospholipid: 1,2-dimyristoyl-*sn*-glycero-3-phosphocholine-d_{72}. *Chem. Phys. Lipids* **24**, 135-147 (1979).
40 Kertz, J. A., Almeida, P. F. F., Frazier, A. A., Berg, A. K. & Hinderliter, A. The cooperative response of synaptotagmin 1 C2A. A hypothesis for a Ca2+-driven molecular hammer. *Biophys. J.* **92**, 1409-1418 (2007).
41 Streicher, W. W. & Makhatadze, G. I. Unfolding thermodynamics of Trp-cage, a 20 residue miniprotein, studied by differential scanning calorimetry and circular dichroism spectroscopy. *Biochemistry* **46**, 2876-2880 (2007).
42 Spolar, R. S., Livingstone, J. R. & Record, M. T. Use of liquid hydrocarbon and amide transfer data to estimate contributions to thermodynamic functions of protein folding from the removal of nonpolar and polar surface from water. *Biochemistry* **31**, 3947-3955 (1992).
43 De Levie, R. Estimating parameter precision in nonlinear least squares with excel's solver. *J. Chem. Educ.* **76**, 1594-1598 (1999).
44 Hill, T. L. *An introduction to statistical thermodynamics*. (General Publishing Company, Ltd, 1986).
45 Damer, C. K. & Creutz, C. E. Calcium-dependent self-association of synaptotagmin I. *J. Neurochem.* **67**, 1661-1668 (1996).
46 Kumar, S., Tsai, C.-J. & Nussinov, R. Maximal stabilities of reversible two-state proteins. *Biochemistry* **41**, 5359-5374 (2002).
47 Privalov, P. L. & Khechinashvili, N. N. A thermodynamic approach to the problem of stabilization of globular protein structure: a calorimetric study. *J. Mol. Biol.* **86**, 665-684 (1974).
48 Gauer, J. W. *Not only the strong survive: weak interactions in peripheral membrane binding proteins* Master of Science thesis, University of Minnesota Duluth, (2011).
49 Rosengarth, A., Rösgen, J., Hinz, H.-J. & Gerke, V. A comparison of the energetics of annexin I and annexin V. *J. Mol. Biol.* **288**, 1013-1025 (1999).
50 Li, J., Motlagh, H. N., Chakuroff, C., Thompson, E. B. & Hilser, V. J. Thermodynamic dissection of the intrinsically disordered N-terminal domain of human glucocorticoid receptor. *J Biol Chem* **287**, 26777-26787 (2012).
51 Sevcsik, E., Trexler, A. J., Dunn, J. M. & Rhoades, E. Allostery in a disordered protein: oxidative modifications to α-synuclein act distally to regulate membrane binding. *J Am Chem Soc* **133**, 7152-7158 (2011).
52 Freiburger, L. A. *et al.* Competing allosteric mechanisms modulate substrate binding in a dimeric enzyme. *Nat Struct Mol Biol* **18**, 288-294 (2011).
53 Garcia-Pino, A. *et al.* Allostery and intrinsic disorder mediate transcription regulation by conditional cooperativity. *Cell* **142**, 101-111 (2010).

54 Khan, S. H., Ling, J. & Kumar, R. TBP binding-induced folding of the glucocorticoid receptor AF1 domain facilitates its interaction with steroid receptor coactivator-1. *PLoS One* **6**, e21939 (2011).
55 Hilser, V. J., Wrabl, J. O. & Motlagh, H. M. Structural and energetic basis of allostery. *Annu Rev Biophys* **41**, 585-609 (2012).
56 Chen, Y. & Barkley, M. D. Toward understanding tryptophan fluorescence in proteins. *Biochemistry* **37**, 9976-9982 (1998).
57 van den Bogaart, G., Meyenberg, K., Diederichsen, U. & Jahn, R. Phosphatidylinositol 4,5-bisphosphate increases the Ca^{2+} affinity of synaptotagmin-1 40-fold. *J. Biol. Chem.* **287**, 16447-16453 (2012).
58 DiAntonio, A., Parfitt, K. D. & Schwarz, T. L. Synaptic transmission persists in synaptotagmin mutants of Drosophila. *Cell* **73**, 1281-1290 (1993).
59 Kyoung, M. *et al.* In vitro system capable of differentiating fast Ca2+-triggered content mixing from lipid exchange for mechanistic studies of neurotransmitter release. *Proc. Natl. Acad. Sci. USA* **108**, 304-313 (2011).
60 Choi, U. B. *et al.* Single-molecule FRET-derived model of the synaptotagmin 1-SNARE fusion complex. *Nat. Struct. Mol. Biol.* **17**, 318-324 (2010).
61 Lai, A. L., Huang, H., Herrick, D. Z., Epp, N. & Cafiso, D. S. Synaptotagmin 1 and SNAREs form a complex that is structurally heterogeneous. *J. Mol. Biol.* **405**, 696-706 (2011).
62 Koh, T. W. & Bellen, H. J. Synaptotagmin I, a Ca2+ sensor for neurotransmitter release. *Trends Neurosci.* **26**, 413-422 (2003).
63 Rizo, J., Chen, X. & Araç, D. Unraveling the mechanisms of synaptotagmin and SNARE function in neurotransmitter release. *Trends Cell Biol.* **16**, 339-350 (2006).
64 Uversky, V. N. Multitude of binding modes attainable by intrinsically disordered proteins: a portrait gallery of disorder-based complexes. *Chem Soc Rev* **40**, 1623-1634 (2011).
65 Paddock, B. E. *et al.* Membrane penetration by synaptotagmin is required for coupling calcium binding to vesicle fusion in vivo. *J. Neurosci.* **31**, 2248-2257 (2011).
66 Blankenship, A. G. & Feller, M. B. Mechanisms underlying spontaneous patterned activity in developing neural circuits. *Nat Rev Neurosci* **11**, 18-29 (2010).
67 Caroni, P., Donato, F. & Muller, D. Structural plasticity upon learning: regulation and functions. *Nat Rev Neurosci* **13**, 478-490 (2012).
68 O'Rourke, N. A., Weiler, N. C., Micheva, K. D. & Smith, S. J. Deep molecular diversity of mammalian synapses: why it matters and how to measure it. *Nat Rev Neurosci* **13**, 365-379 (2012).
69 Changeux, J.-P., Thiéry, J., Tung, Y. & Kittel, C. On the cooperativity of biological membranes. *Proc Natl Acad Sci USA* **57**, 335-341 (1967).
70 Hinderliter, A. K., Almeida, P. F. F., Biltonen, R. L. & Creutz, C. E. Membrane domain formation by calcium-dependent, lipid-binding proteins: insights from the C2 motif. *Biochim Biophys Acta* **1448**, 227-235 (1998).
71 Simons, K. & Toomre, D. Lipid rafts and signal transduction. *Nat Rev Mol Cell Biol* **1**, 31-39 (2000).

72 Simons, K. & Sampaio, J. L. Membrane organization and lipid rafts. *Cold Spring Harb Perspect Biol* **3**, a004697 (2011).
73 Almeida, P. F. F., Pokorny, A. & Hinderliter, A. Thermodynamics of membrane domains. *Biochim Biophys Acta* **1720**, 1-13 (2005).
74 Changeux, J.-P. & Danchin, A. Selective stabilisation of developing synapses as a mechanism for the specification of neuronal networks. *Nature* **264**, 705-712 (1976).
75 Fukuda, M. *et al.* Role of conserved WHXL motif in the C terminus of synaptotagmin in synaptic vesicle docking. *Proc Natl Acad Sci USA* **97**, 14715-14719 (2000).
76 Lynch, K. L. *et al.* Synaptotagmin-1 utilizes membrane bending and SNARE binding to drive fusion pore expansion. *Mol Biol Cell* **19**, 5093-5103 (2008).
77 Sørensen, J. B. Conflicting views on the membrane fusion machinery and the fusion pore. *Annu Rev Cell Dev Biol* **25**, 513-537 (2009).
78 Fealey, M. E. *et al.* Negative coupling as a mechanism for signal propagation between C2 domains of synaptotagmin I. *PLoS One* **7**, e46748 (2012).
79 Xu, T. *et al.* Rapid formation and selective stabilzation of synapses for enduring motor memories. *Nature* **462**, 915-919 (2009).
80 Wong, R. O. & Ghosh, A. Activity-dependent regulation of dendritic growth and patterning. *Nat Rev Neurosci* **3**, 803-812 (2002).
81 Chen, J. W., Romero, P., Uversky, V. N. & Dunker, A. K. Conservation of intrinsic disorder in protein domains and families: I. A database of conserved predicted disordered regions. *J Proteome Res* **5**, 879-887 (2006).
82 Chen, J. W., Romero, P., Uversky, V. N. & Dunker, A. K. Conservation of intrinsic disorder in protein domains and families: II. functions of conserved disorder. *J Proteome Res* **5**, 888-898 (2006).
83 Monod, J., Wyman, J. & Changeux, J.-P. On the nature of allosteric transitions: a plausible model. *J Mol Biol* **12**, 88-118 (1965).
84 Tobi, D. & Bahar, I. Structural changes involved in protein binding correlate with intrinsic motions of proteins in the unbound state. *Proc Natl Acad Sci USA* **102**, 18908-18913 (2005).
85 Bahar, I., Chennubhotla, C. & Tobi, D. Intrinsic dynamics of enzymes in the unbound state and relation to allosteric regulation. *Curr Opin Struct Biol* **17**, 633-640 (2007).
86 Koshland, D. E., Némethy, G. & Filmer, D. Comparison of experimental binding data and theoretical models in proteins containing subunits. *Biochemistry* **5**, 365-385 (1966).
87 James, L. C. & Tawfik, D. S. Conformational diversity and protein evolution--a 60-year-old hypothesis revisited. *Trends Biochem Sci* **28**, 361-368 (2003).
88 Pang, Z. P. & Südhof, T. C. Cell biology of Ca2+-triggered exocytosis. *Curr Opin Cell Biol* **22**, 496-505 (2010).
89 Südhof, T. C. Synaptotagmins: why so many? *J Biol Chem* **277**, 7629-7632 (2002).
90 Mahal, L. K., Sequeira, S. M., Gureasko, J. M. & Söllner, T. H. Calcium-independent stimulation of membrane fusion and SNAREpin formation by synaptotagmin I. *J Cell Biol* **158**, 273-282 (2002).

91 Stein, A., Radhakrishnan, A., Riedel, D., Fasshauer, D. & Jahn, R. Synaptotagmin activates membrane fusion through a Ca2+-dependent trans interaction with phospholipids. *Nat. Struct. Mol. Biol.* **14**, 904-911 (2007).
92 Vennekate, W. *et al.* Cis- and trans-membrane interactions of synaptotagmin-1. *Proc Natl Acad Sci USA* **109**, 11037-11042 (2012).
93 Wang, Z., Liu, H., Gu, Y. & Chapman, E. R. Reconstituted synaptotagmin I mediates vesicle docking, priming, and fusion. *J Cell Biol* **195**, 1159-1170 (2011).
94 Romero, P. *et al.* Sequence complexity of disordered protein. *Proteins* **42**, 38-48 (2001).
95 Dyson, H. J. & Wright, P. E. Intrinsically unstructured proteins and their functions. *Nat Rev Mol Cell Biol* **6**, 197-208 (2005).
96 Mittag, T., Kay, L. E. & Forman-Kay, J. D. Protein dynamics and conformational disorder in molecular recognition. *J Mol Recognit* **23**, 105-116 (2010).
97 Uversky, V. N., Oldfield, C. J. & Dunker, A. K. Showing your ID: intrinsic disorder as an ID for recognition, regulation and cell signaling. *J Mol Recognit* **18**, 343-384 (2005).
98 Yoshihara, M. & Littleton, J. T. Synaptotagmin I functions as a calcium sensor to synchronize neurotransmitter release. *Neuron* **36**, 897-908 (2002).
99 Fealey, M. E. & Hinderliter, A. Allostery and instability in the functional plasticity of synaptotagmin I. *Commun Integr Biol* **6**, e22830 (2013).
100 Liu, T., Whitten, S. T. & Hilser, V. J. Functional residues serve a dominant role in mediating the cooperativity of the protein ensemble. *Proc Natl Acad Sci USA* **104**, 4347-4352 (2007).
101 Gauer, J. W. *et al.* Membrane modulates affinity for calcium ion to create an apparent cooperative binding response by annexin a5. *Biophys J* **In press** (2013).
102 Prilusky, J. *et al.* FoldIndex: a simple tool to predict whether a given protein sequence is intrinsically unfolded. *Bioinformatics* **21**, 3435-3438 (2005).
103 Kelley, L. A. & Sternberg, M. J. Protein structure prediction on the Web: a case study using the Phyre server. *Nat Protoc* **4**, 363-371 (2009).
104 Peng, K., Radivojac, P., Vucetic, S., Dunker, A. K. & Obradovic, Z. Length-dependent prediction of protein intrinsic disorder. *BMC Bioinformatics* **7**, 208 (2006).
105 Peng, K. *et al.* Optimizing long intrinsic disorder predictors with protein evolutionary information. *J Bioinform Comput Biol* **3**, 35-60 (2005).
106 Zhang, Y. I-TASSER server for protein 3D structure prediction. *BMC Bioinformatics* **9**, 1-8 (2008).
107 Dunker, A. K. *et al.* Intrinsically disordered protein. *J Mol Graph Model* **19**, 26-59 (2001).
108 Perin, M. S., Brose, N., Jahn, R. & Südhof, T. C. Domain structure of synaptotagmin (p65). *J Biol Chem* **266**, 623-629 (1991).
109 Vacic, V. *et al.* Characterization of molecular recognition features, MoRFs, and their binding partners. *J Proteome Res* **6**, 2351-2366 (2007).
110 Shin, O. H., Xu, J., Rizo, J. & Südhof, T. C. Differential but convergent functions of Ca2+ binding to synaptotagmin-1 C2 domains mediate neurotransmitter release. *Proc Natl Acad Sci USA* **106**, 16469-16474 (2009).

111 Shao, X., Fernandez, I., Südhof, T. C. & Rizo, J. Solution structures of the Ca2+-free and Ca2+-bound C2A domain of synaptotagmin I: does Ca2+ induce a conformational change? *Biochemistry* **37**, 16106-16115 (1998).
112 Wrabl, J. O. *et al.* The role of protein conformational fluctuations in allostery, function, and evolution. *Biophys Chem* **159**, 129-141 (2011).
113 Bai, J., Wang, P. & Chapman, E. R. C2A activates a cryptic Ca(2+)-triggered membrane penetration activity within the C2B domain of synaptotagmin I. *Proc Natl Acad Sci USA* **99**, 1665-1670 (2002).